ANTARCTIC SCIENCE NEWS

News date: 27.6.2016 compiled by Dr. Alvarinho J. Luis

Super-slow circulation allowed world's oceans to store huge amounts of carbon during last ice age

The way the ocean transported heat, nutrients and carbon dioxide at the peak of the last ice age, about 20,000 years ago, is significantly different than what has previously been suggested, according to two new studies. The findings suggest that the colder ocean circulated at a very slow rate, which enabled it to store much more carbon for much longer than the modern ocean.

The way the ocean transported heat, nutrients and carbon dioxide (CO_2) at the peak of the last ice age, about 20,000 years ago, is significantly different than what has previously been suggested, according to two new studies. The findings suggest that the colder ocean circulated at a very slow rate, which enabled it to store much more carbon for much longer than the modern ocean.

Using the information contained within the shells of tiny animals known as foraminifera, the researchers, led by the University of Cambridge, looked at the characteristics of the seawater in the Atlantic Ocean during the last ice age, including its ability to store carbon. Since atmospheric CO_2 levels during the period were about a third lower than those of the pre-industrial atmosphere, the researchers were attempting to find if the extra carbon not present in the atmosphere was stored in the deep ocean instead.

They found that the deep ocean circulated at a much slower rate at the peak of the last ice age than had previously been suggested, which is one of the reasons why it was able to store much more carbon for much longer periods. That carbon was accumulated as organisms from the surface ocean died and sank into the deep ocean where their bodies dissolved, releasing carbon that was in effect 'trapped' there for thousands of years. Their results are reported in two separate papers in *Nature Communications*.

The ability to reconstruct past climate change is an important part of understanding why the climate of today behaves the way it does. It also helps to predict how the planet might respond to changes made by humans, such as the continuing emission of large quantities of CO_2 into the atmosphere.

The world's oceans work like a giant conveyor belt, transporting heat, nutrients and gases around the globe. In today's oceans, warmer waters travel northwards along currents such as the Gulf Stream from the equatorial regions towards the pole, becoming saltier, colder and denser as they go, causing them to sink to the bottom. These deep waters flow into the ocean basins, eventually ending up in the Southern Ocean or the North Pacific Ocean. A complete loop can take as long as 1000 years.

During the period we looked at, large amounts of carbon were likely transported from the surface ocean to the deep ocean by organisms as they died, sunk and dissolved said Emma Freeman, the lead author of one of the papers. This process released the carbon the organisms contained into the deep ocean waters, where it was trapped for thousands of years, due to the very slow circulation.

Freeman and her co-authors used radiocarbon dating, a technique that is more commonly used by archaeologists, in order to determine how old the water was in different parts of the ocean. Using the radiocarbon information from tiny shells of foraminifera, they found that carbon was stored in the slowly-circulating deep ocean.

In a separate study led by Jake Howe, also from Cambridge Univ., researchers studied the neodymium isotopes contained in the foraminifera shells, a method which works like a dye tracer, and came to a similar conclusion about the amount of carbon the ocean was able to store.

We found that during the peak of the last ice age, the deep Atlantic Ocean was filled not just with southern-sourced waters as previously thought, but with northern-sourced waters as well, said Howe.

What was previously interpreted to be a layer of southern-sourced water in the deep Atlantic during the last ice age was in fact shown to be a mixture of slowly circulating northern- and southern-sourced waters with a large amount of carbon stored in it.

Our research looks at a time when the world was much colder than it is now, but it's still important for understanding the effects of changing ocean circulation, said Freeman. We need to understand the dynamics of the ocean in order to know how it can be affected by a changing climate.

1. **J. N. W. Howe, A. M. Piotrowski, T. L. Noble, S. Mulitza, C. M. Chiessi, G. Bayon.** North Atlantic Deep Water Production during the Last Glacial Maximum**. *Nature Communications*, 2016; 7: 11765 DOI: 10.1038/ncomms11765**
2. **E. Freeman, L. C. Skinner, C. Waelbroeck, D. Hodell.** Radiocarbon evidence for enhanced respired carbon storage in the Atlantic at the Last Glacial Maximum**. *Nature Communications*, 2016; 7: 11998 DOI: 10.1038/ncomms11998**

Source: University of Cambridge

pdf reprints follows ....

nature COMMUNICATIONS

ARTICLE

Received 27 Oct 2015 | Accepted 27 Apr 2016 | Published 3 Jun 2016

DOI: 10.1038/ncomms11765 OPEN

North Atlantic Deep Water Production during the Last Glacial Maximum

Jacob N.W. Howe[1], Alexander M. Piotrowski[1], Taryn L. Noble[1,2], Stefan Mulitza[3], Cristiano M. Chiessi[4] & Germain Bayon[5]

Changes in deep ocean ventilation are commonly invoked as the primary cause of lower glacial atmospheric CO_2. The water mass structure of the glacial deep Atlantic Ocean and the mechanism by which it may have sequestered carbon remain elusive. Here we present neodymium isotope measurements from cores throughout the Atlantic that reveal glacial–interglacial changes in water mass distributions. These results demonstrate the sustained production of North Atlantic Deep Water under glacial conditions, indicating that southern-sourced waters were not as spatially extensive during the Last Glacial Maximum as previously believed. We demonstrate that the depleted glacial $\delta^{13}C$ values in the deep Atlantic Ocean cannot be explained solely by water mass source changes. A greater amount of respired carbon, therefore, must have been stored in the abyssal Atlantic during the Last Glacial Maximum. We infer that this was achieved by a sluggish deep overturning cell, comprised of well-mixed northern- and southern-sourced waters.

[1] Department of Earth Sciences, University of Cambridge, Cambridge CB2 3EQ, UK. [2] Institute for Marine and Antarctic Studies (IMAS), University of Tasmania, Hobart, Tasmania 7001, Australia. [3] MARUM-Center for Marine Environmental Sciences, University of Bremen, Leobener Strasse, D-28359 Bremen, Germany. [4] School of Arts, Sciences and Humanities, University of São Paulo, Av. Arlindo Bettio 1000, CEP03828-000 São Paulo SP, Brazil. [5] Institut Français de Recherche pour l'Exploitation de la Mer (IFREMER), Unité de Recherche Géosciences Marines, F-29280 Plouzané, France. Correspondence and requests for materials should be addressed to J.N.W.H. (email: jacob.howe@cantab.net).

Changes in Atlantic Meridional Overturning Circulation are important in controlling glacial–interglacial climatic shifts due to their role in regulating heat transport in the surface ocean and carbon storage in the deep ocean[1,2]. Nutrient-based proxy reconstructions suggest that overturning circulation in the Atlantic during the Last Glacial Maximum (LGM) was different to that of the modern ocean[3–5]. These nutrient proxy reconstructions are often interpreted as indicating that during the LGM North Atlantic Deep Water (NADW) shoaled to form Glacial North Atlantic Intermediate Water (GNAIW) and was completely replaced by southern-sourced water in the deep Atlantic (>2.5 km)[6,7]. However, elucidation of the water mass distribution in such reconstructions is complicated by the fact that the nutrient content of deep waters may vary independently of their source and dynamics[8]; meanwhile, modelling studies of glacial Atlantic overturning have produced conflicting results[9].

In the modern ocean Antarctic Bottom Water (AABW), which is formed in the high latitude Southern Ocean, represents a major inefficiency in the biological pump—the name given to the biologically mediated processes which sequester carbon in the deep ocean. In this region, deep waters are upwelled to the surface, allowing dissolved carbon to be outgassed to the atmosphere, but these waters sink again before their nutrient load can be fully consumed by marine organisms, thus they are said to have a high-preformed nutrient concentration[10]. The formation of NADW and AABW, and their resultant proportions in the deep ocean thus controls the preformed nutrient concentration of the deep ocean, which, in part, controls atmospheric pCO_2 (ref. 11). Ice core records show that atmospheric CO_2 concentrations rose by $\sim$90 p.p.m. between the LGM and the Holocene[12]. However, considered in isolation, the replacement of high-preformed nutrient AABW with low-preformed nutrient NADW, which has been suggested to have occurred across the last deglaciation, would have increased the efficiency of the biological pump and thereby decreased atmospheric CO_2 (refs 11,13). If our current understanding of glacial–interglacial circulation changes is correct then other parts of the carbon cycle must have counteracted the effects of switching from the GNAIW to NADW mode of deep water formation across the deglaciation. Alternatively, nutrient proxy reconstructions of the Atlantic may be recording carbon cycle changes rather than differences in water mass sourcing.

Neodymium isotopes are a water mass tracer independent of biological processes, allowing deconvolution of changes in water mass sourcing and nutrient regeneration[14]. Modern NADW has a characteristic ε_{Nd} value (normalized $^{143}Nd/^{144}Nd$ ratio in parts per ten thousand) of -13.5 (ref. 15) while seawater in the deep Southern Ocean shows ε_{Nd} values around -8.5 (ref. 16), because it has a greater proportion of Pacific Deep Water (PDW) which has an ε_{Nd} of -3.5 (ref. 17). Away from continental margins water masses throughout the deep ocean reflect the quasi-conservative mixing of these deep water masses[14]. Planktic foraminifera from sea-floor sediment cores have been shown to successfully preserve bottom water ε_{Nd}, thereby offering an archive of past seawater ε_{Nd} (ref. 18).

Here we present Holocene and LGM seawater ε_{Nd} reconstructions, based on foraminiferal ε_{Nd} measurements from 24 cores (Supplementary Table 1, Supplementary Fig. 1) spanning from 46° S to 40° N in the Atlantic Ocean. These reconstructions are used to decipher the nature of changes in Atlantic water mass distributions between glacial and interglacial conditions. Although the LGM reconstruction shows more radiogenic neodymium isotope values than the Holocene profile, the observation of less radiogenic values in the deep North Atlantic than the deep South Atlantic indicates that NADW was produced under glacial conditions. When compared with benthic foraminiferal carbon isotope values, the neodymium isotope measurements reveal that more respired organic carbon was stored in the deep Atlantic Ocean during the LGM than in the Holocene.

Results

Core top foraminiferal ε_{Nd} versus seawater ε_{Nd}. Figure 1 cross plots the Holocene foraminiferal ε_{Nd} values (Supplementary Tables 2 and 3) against the nearest available published seawater ε_{Nd} measurements. Data points were only included in the cross plot if the seawater measurements were within both 10° of latitude and longitude and within 500 m depth of the core site. Most of the data points on the cross plot are within error of the 1:1 line, indicating that foraminifera are faithfully preserving seawater ε_{Nd}. Despite the distance criteria outlined above being applied, the three data points which are outside of error of the 1:1 line are likely due to the seawater data not being of sufficiently close proximity to represent the water mass bathing the core sites. This effect is likely to be particularly prominent in site locations that are near water mass boundaries.

Holocene Atlantic ε_{Nd} reconstruction. We gridded our Holocene foraminiferal ε_{Nd} measurements (Supplementary Table 2) with suitable published data (Fig. 2c). The published data includes results from measurements made on foraminifera, fish debris, high resolution crusts and leachates (Supplementary Tables 3 and 4). As some measurements made on leachates have been shown to be susceptible to contamination by the detrital fraction[19,20], results from sites where the core top leachate ε_{Nd} values deviated significantly from nearby seawater values were excluded from the reconstruction. The data points included from the crusts BM1969.05 and TR079 D-14 (Supplementary Table 4) were dated outside of the definition of the LGM used for selecting sediment core data (23–18 ka); however, the records from these crusts were used to argue for the stability of seawater ε_{Nd} across glacial–interglacial cycles in their respective locations[21]. The slightly older glacial data points from these crusts were therefore deemed appropriate for inclusion in the LGM time slice.

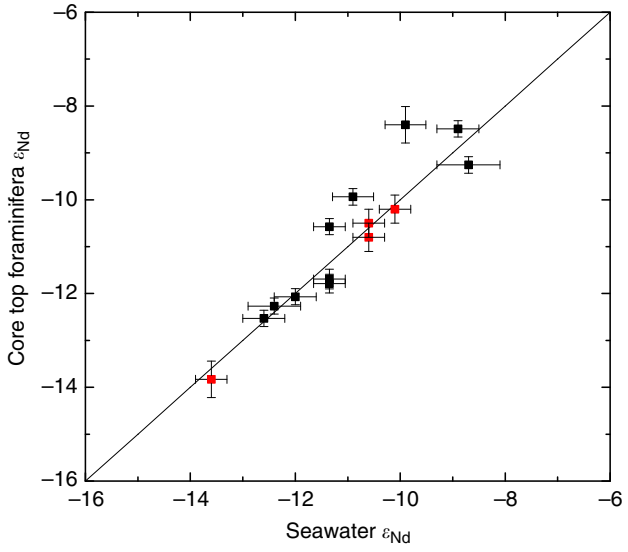

Figure 1 | Core top foraminiferal ε_{Nd} versus seawater ε_{Nd}. Modern open Atlantic seawater[15,16,55,56] ε_{Nd} cross plotted against Holocene Atlantic ε_{Nd} measurements made on uncleaned planktic foraminifera in this work (black squares; Supplementary Table 2) together with previously reported foraminiferal values used in this work (red squares; Supplementary Table 3)[18,56]. Error bars are 2σ external errors. A 1:1 line is also plotted.

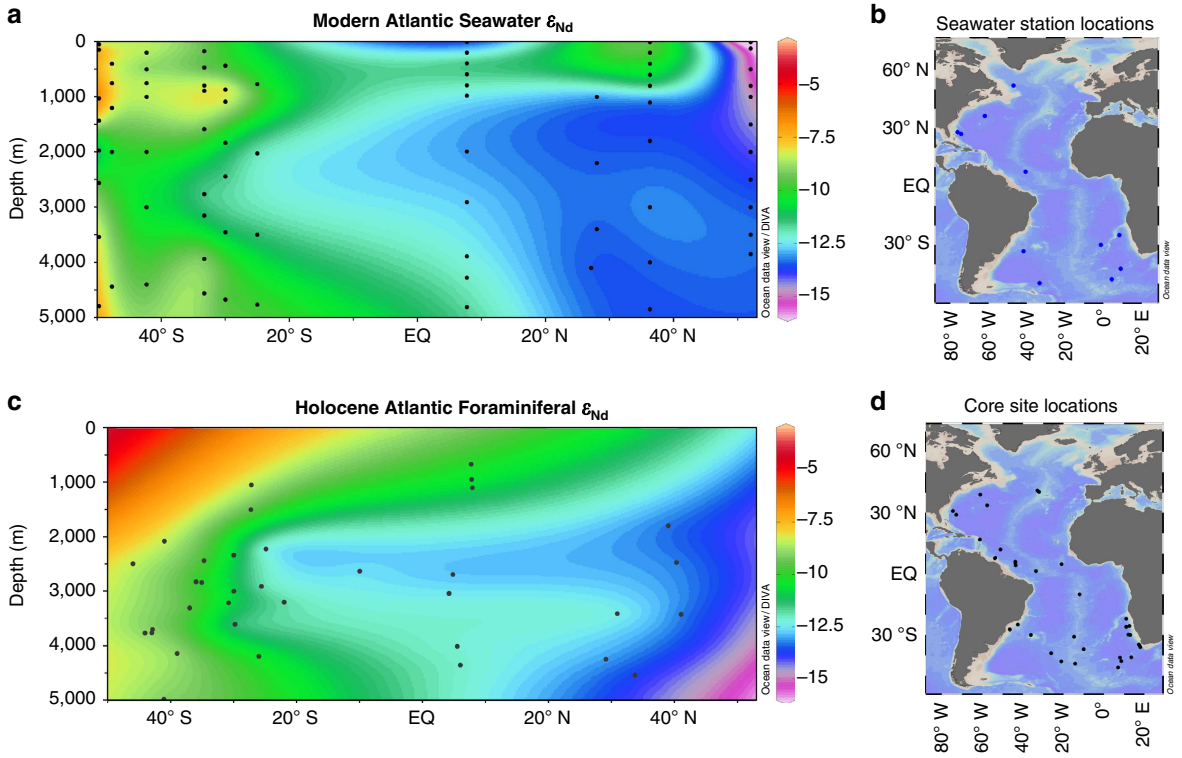

Figure 2 | Atlantic seawater ε_{Nd} and Holocene ε_{Nd} reconstruction. (**a**) Modern seawater ε_{Nd} profile from 50° S to 53° N for the western Atlantic and the eastern Atlantic Ocean south of the Walvis Ridge with data points indicated by large black dots[15,16,55]. (**b**) Map showing location of seawater ε_{Nd} profiles. (**c**) Reconstruction of Holocene Atlantic ε_{Nd} with data points indicated by large black dots (data is listed in Supplementary Tables 2,3 and 4). (**d**) Map showing location of sites used in the Holocene and LGM reconstructions. Figure created using Ocean Data View software[22].

DIVA gridding was performed using Ocean Data View[22] with the 'signal-to-noise ratio' variable set to a value of 25. This variable determines how much a single data point is able to influence the overall plot and this level was chosen to reduce the influence of single data points, as was done by Curry and Oppo[4].

The Holocene reconstruction shows the most unradiogenic ε_{Nd} values, around -13, below 1,500 m at the northernmost extent of the plot (Fig. 2c). These values become more radiogenic to the south, with the greatest propagation of this unradiogenic signal centred at 2,000–4,000 m water depth. This is surrounded by areas with more radiogenic ε_{Nd} values, from -8 to -10, at all depths south of 25° S; below 4,000 m from 25° S to the equator; and above 1,500 m at all latitudes. Although the data set is not as extensive as that used in $\delta^{13}C$ reconstructions[4], this reconstruction replicates the salient features of the seawater ε_{Nd} (Fig. 2a). The only significant mismatches are above 1,000 m at all latitudes and below 4,000 m north of 40° N; in these regions the gridding procedure extrapolates from the nearest data point to the edge of the profile due to a lack of data based constraints. These areas should therefore be interpreted with caution and for this reason the depth range of 0–1,000 m is excluded from later reconstructions.

Last Glacial Maximum Atlantic ε_{Nd} reconstruction. The good correlation between seawater ε_{Nd} and the salinity profile of the modern Atlantic[23] demonstrates that the modern seawater ε_{Nd} profile is the result of mixing between northern- and southern-sourced water masses. Collectively, these observations provide confidence that this selection of cores can be used to constrain past Atlantic water mass distributions below 1,000 m. The LGM ε_{Nd} reconstruction (Fig. 3b) shows the most unradiogenic values around -12.5 between 1,500 and 2,000 m extending from the

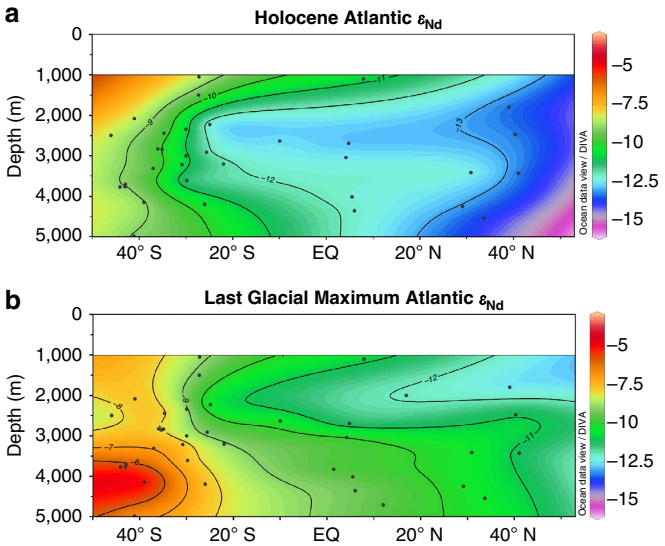

Figure 3 | Holocene and LGM Atlantic ε_{Nd} reconstructions. (**a**) Holocene and (**b**) LGM (23–18 ka) reconstructions of ε_{Nd} of the Atlantic Ocean from 50° S to 53° N measured on uncleaned foraminifera in this study and published authigenic data (Supplementary Tables 2,3 and 4)[18,21,25,26,32,56–59]. Core sites are given by the black dots; locations are plotted in Fig. 2d and Supplementary Fig. 1. Depths from 0 to 1,000 m have been left blank due to a lack of data. Figure created using Ocean Data View software[22].

North Atlantic to ~10° N which then transition to values around -8 at 40° S. In contrast, the deep North Atlantic is occupied by a homogeneous water mass with an ε_{Nd} around -10.5; ε_{Nd} values become more radiogenic to the south, reaching -5.5 at 45° S.

The largest differences between the LGM and modern Atlantic profiles occur below 2,500 m (Fig. 3); the deep North Atlantic shifts from ε_{Nd} values around −10.5 in the glacial to −13.5 in the modern ocean, whilst the deep South Atlantic shifts from −5.5 to −8.5. This coherent spatial pattern of changes in ε_{Nd} values in the Atlantic between the LGM and the Holocene (Fig. 3b) is consistent with a change in water mass advection and indicates there was a greater influence of southern-sourced waters in the deep Atlantic under glacial conditions.

Discussion

The change observed in the deep South Atlantic between the LGM and Holocene (Fig. 3) is consistent with a lower flux of NADW into the Southern Ocean under cooler, glacial conditions[24,25]. This lower flux of NADW resulted in the deep Southern Ocean being filled with a greater proportion of water of Pacific and Indian Ocean origin that was more radiogenic in composition than Atlantic-sourced deep water[26–28]. The deep South Atlantic, however, remained less radiogenic than the deep Pacific[26,28], requiring a source of unradiogenic neodymium to the deep South Atlantic under glacial conditions. Furthermore, the deep North Atlantic was less radiogenic than the deep South Atlantic during the LGM (Fig. 3b); this implies that northern-sourced water with its unradiogenic ε_{Nd} must have been exported to abyssal depths under glacial climate conditions. The mixing of GNAIW with denser southern-sourced waters is deemed an unlikely explanation given the large amount of energy required to mix these intermediate waters down to abyssal depths in the North Atlantic. Rather, these observations suggest that two glacial North Atlantic-sourced water masses existed during the LGM: GNAIW at depths above 2,500 m and denser Glacial NADW (GNADW)[29] below 2,500 m.

The inference of a lower flux of GNADW under glacial conditions[24] than NADW in the Holocene resulting in a more radiogenic composition of Glacial AABW (GAABW) than AABW would cause the deep Atlantic to exhibit more radiogenic ε_{Nd} values without a change in the water mass mixing proportions in the deep Atlantic. By taking this end-member change of deep southern-sourced water ε_{Nd} into account, however, our results can be used to calculate the proportion of the Atlantic ventilated by NADW (%NADW) both in the Holocene and during the LGM (Supplementary Table 5), and thus elucidate changes in water mass mixing proportions from the effect of the change in the AABW end-member composition. In each case three end-members were required; namely NADW; AABW and Antarctic Intermediate Water, or their glacial counterparts (Supplementary Fig. 2). A binary mixing calculation was performed between a northern- and a southern-sourced water mass at each core site using equation (1). The choice of southern-sourced water varied with depth and latitude according to the observed boundary between Antarctic Intermediate Water and Lower Circumpolar Deep Water as defined by a salinity of 34.7 psu (ref. 30) and the gradient in neodymium concentration (but not ε_{Nd}) between them in the Atlantic sector of the modern Southern Ocean[16].

$$\%\,\mathrm{NADW} = \frac{[\mathrm{Nd}]_{SSW}(\varepsilon_{Nd(NADW)} - \varepsilon_{Nd(SSW)})}{[\mathrm{Nd}]_{NADW}\varepsilon_{Nd(NADW)} - [\mathrm{Nd}]_{SSW}\varepsilon_{Nd(SSW)} - \varepsilon_{Nd}\varepsilon_{Nd(NADW)} + \varepsilon_{Nd(SSW)}\varepsilon_{Nd}} \times 100 \quad (1)$$

The modern seawater ε_{Nd} and [Nd] end-member values were taken from published seawater data (Supplementary Fig. 2). For the glacial ocean, the ε_{Nd} and [Nd] of NADW and PDW were kept constant; support for the stability of the ε_{Nd} of both comes from crust data[31] whilst there is, at present, no proxy for past neodymium concentration available. The more radiogenic ε_{Nd} of GAABW was taken from a South Atlantic record of benthic foraminifera[32] and the concentration calculated by conservative mixing of NADW and PDW (ref. 16). Unlike records from the deep South Atlantic[26,32], the new intermediate depth glacial foraminiferal ε_{Nd} data from the South Atlantic measured in this work exhibit no changes between the LGM and the Holocene (GeoB2107-3 and GeoB2104-3; Supplementary Table 2), so the neodymium composition of Glacial Antarctic Intermediate Water was assumed to be the same as in the modern ocean. This observation clearly demonstrates that the intermediate and deep South Atlantic were isotopically distinct in terms of neodymium during the LGM, reinforcing the need for two distinct southern-sourced end-member water masses in the mixing calculations.

Figure 4 shows the %NADW values calculated for the Holocene and LGM Atlantic gridded into meridional sections using the same technique employed for the ε_{Nd} data profiles plotted in Fig. 2. In the LGM ε_{Nd} profile (Fig. 3b), the most radiogenic values, around −5.5, are observed at 4,000 m depth in the South Atlantic, whereas less radiogenic values, around −6.5, are seen at ~5,000 m at the same latitude. The more radiogenic values come from the Mid-Atlantic Ridge; the less radiogenic from the Cape Basin, which lies to the east of the Mid-Atlantic Ridge. The ε_{Nd} difference between these sites likely reflects a longitudinal mixing gradient between radiogenic, Pacific-derived, circumpolar waters[28] and less radiogenic North Atlantic derived waters[25]. A similar phenomenon is seen in modern seawater data from the South Atlantic although the offset is less pronounced[16]. The results from the deep Cape Basin[26] were, therefore, excluded from the mixing proportion plots in Fig. 4 as the longitudinal gradient in ε_{Nd} observed in the deep South Atlantic obscures the latitudinal mixing gradient which is the primary interest here.

The gridded profile of the Holocene %NADW results (Fig. 4a) shows the Atlantic north of 20° N and below 1,500 m depth is mostly (>90%) NADW. %NADW decreases at all depths to the

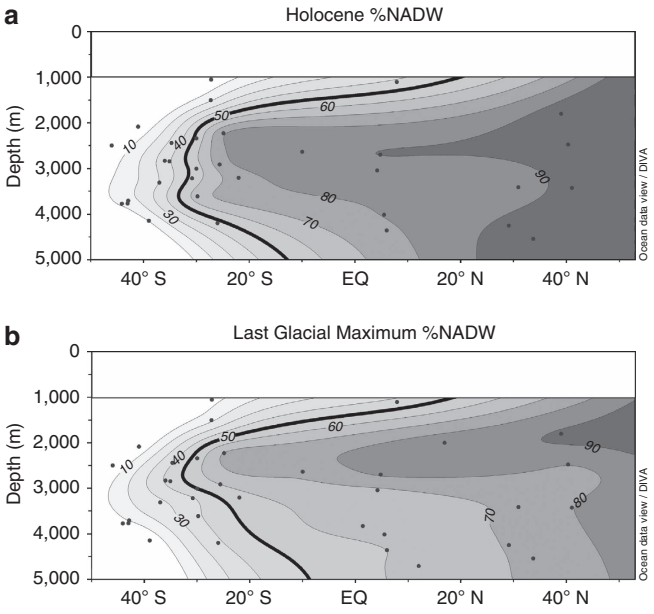

Figure 4 | Holocene and LGM NADW percentage. NADW percentage (%NADW) calculated for the Atlantic Ocean from 50° S to 53° N in the (**a**) Holocene and during the (**b**) LGM (23–18 ka) using authigenic ε_{Nd}. Depths from 0 to 1,000 m have been left blank due to a lack of data. Figure created using Ocean Data View software[22].

south, with the 50% mixing line occurring near 10° S at 5,000 m, but not until 30° S from 2,000 to 4,000 m. The LGM %NADW contours, including the 50% contour, (Fig. 4b) are similar to the Holocene profile above 2,500 m (Fig. 4a). The greatest difference between the two plots occurs below 2,500 m in the North Atlantic, which has significantly less NADW in the LGM profile (55–80% NADW) than in the Holocene profile (>90% NADW). From this observation it is clear that there was a greater proportion of southern-sourced waters in the deep Atlantic during the LGM than in the Holocene; however, it is also clear that the deep Atlantic was not occupied solely by southern-sourced waters during the LGM.

Although changes in the proportion of NADW in the deep Atlantic between glacial and interglacial conditions are the simplest explanation for the results in Figs 3 and 4, other alternatives must be considered. The sensitivity of the calculated %NADW for the glacial deep Bermuda Rise ε_{Nd} of −10.4 (OCE326-GGC6; 33.7° N, 57.6° W, 4,540 m)[18] to the neodymium composition of end-member water masses is shown in Fig. 5. The ε_{Nd} of AABW, considered to be known with reasonable confidence[32], was held constant. The ε_{Nd} of GNADW was varied from a near maximum possible value of −10.5 to a minimum of −16.5, similar to the least radiogenic value of −16 that was used in similar calculations performed for a nearby site[33]. As the %NADW result is dependent on the relative neodymium concentrations of the northern and southern end-members, the ratio of $[Nd]_{GNADW}$ to $[Nd]_{GAABW}$ was varied from 0.2 to 1. The latter value was used in similar calculations performed for a South Atlantic site[32] and is used as an upper limit in this work as ratios >1 would require more neodymium dissolved in the deep Atlantic than the deep Pacific, a situation that is not consistent with the observation that neodymium concentrations increase with water mass age in the modern ocean[34].

Using the glacial end-member values assigned in Fig. 4, the deep Bermuda Rise site was calculated to be bathed by 72% NADW during the LGM (black box, Fig. 5). In contrast an $\varepsilon_{Nd(GNADW)}$ of −10.5 and concentration ratio of 0.2 yields nearly

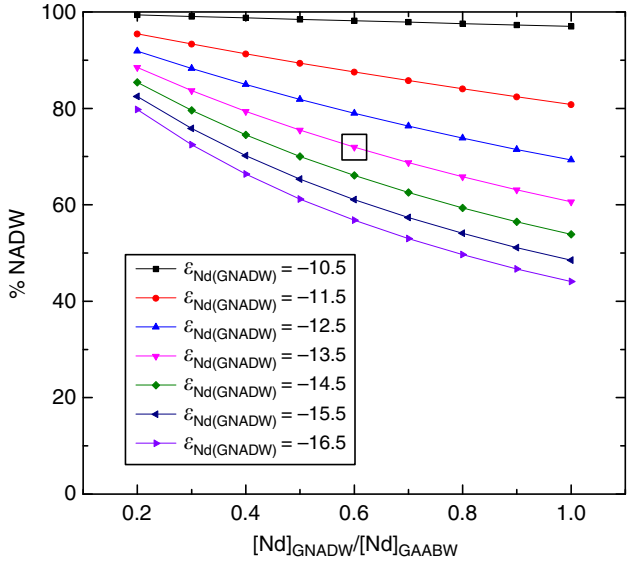

Figure 5 | Sensitivity test of NADW percentage calculation. Results of the sensitivity tests performed on the %NADW calculated for the Bermuda Rise ε_{Nd} of −10.4 during the LGM (OCE326-GGC6; 33.7° N, 57.6° W, 4,540 m)[18]. $\varepsilon_{Nd(GAABW)}$ was held constant at −5.5 (ref. 32), whilst $\varepsilon_{Nd(GNADW)}$ and the ratio of $[Nd]_{GNADW}$ to $[Nd]_{GAABW}$ were varied as shown. The result from end-members used in Fig. 4 ($\varepsilon_{Nd(GNADW)} = -13.5$ and $[Nd]_{GNADW}/[Nd]_{GAABW} = 0.60$) is highlighted by a black box.

100% NADW, whilst an $\varepsilon_{Nd(GNADW)}$ of −16.5 and a concentration ratio of 1.0 means just 44% NADW is required to explain the ε_{Nd} observed at the Bermuda Rise during the LGM. Although the resultant uncertainty in the %NADW at the Bermuda Rise of ±28% is significant, all end-member configurations yield %NADW in the glacial deep North Atlantic values >44%. This is a robust finding that directly contradicts the notion that the deep Atlantic was dominated by southern-sourced waters during the LGM. Furthermore, the lower estimate of 44% is deemed unlikely to be realistic as less radiogenic $\varepsilon_{Nd(NADW)}$ values appear restricted to interstadials, and have been interpreted as pulses of Labrador Sea Water formation during these warm intervals[33] or unradiogenic weathering pulses during ice sheet retreat[35]. Rather, most evidence suggests that $\varepsilon_{Nd(GNADW)}$ values were similar to or slightly more radiogenic than NADW in the modern Atlantic[21] yielding higher %NADW values (Fig. 5). The influence of analytical error on the calculated %NADW values is small; using the external error bounds of 0.5 epsilon units[18] gives a range of 67–77% NADW at the deep Bermuda Rise during the LGM.

Although these uncertainties do limit the certainty of the exact proportion of the deep Atlantic that was ventilated by northern-sourced waters during the LGM, the need for Glacial NADW appears inescapable. If localized processes, such as boundary exchange, were controlling the glacial ε_{Nd} profile, one would expect to see a heterogeneous profile controlled by regional detrital inputs. Furthermore, modelling studies have shown that boundary exchange processes are not able to explain the magnitude of the observed glacial–interglacial shifts in deep ocean ε_{Nd} and thus changes in water mass advection must be invoked to explain them[36]. Reconstructions of glacial deep water mass ventilation from radiocarbon[37], and carbonate ion concentration from B/Ca[38,39] also show a younger, better ventilated, water mass in the deep North Atlantic than the deep South Atlantic. These proxies, therefore, also provide evidence for a significant proportion of northern-sourced deep waters in the deep North Atlantic during the LGM, supporting the results shown in Fig. 4.

Reconciling the glacial ε_{Nd} values in the Atlantic with nutrient proxy based reconstructions requires a greater amount of respired organic carbon in the deep glacial Atlantic relative to the modern situation[4,8]. Circulation versus biological sources of carbon can be differentiated by cross plots of ε_{Nd} against benthic foraminiferal $\delta^{13}C$ for the Holocene and LGM Atlantic (Fig. 6). Deep water mass mixing end-members were ascribed to each plot as detailed in the Supplementary Information. The South Atlantic foraminiferal values (grey regions Fig. 6) were corrected for the Mackensen Effect, the phenomenon where benthic foraminifera display $\delta^{13}C$ values lower than that of the overlying deep water due to a phytodetrital layer of light organic carbon on the sea floor[40]. The composition of NADW is similar in the Holocene and LGM cross plots with $\delta^{13}C$ and ε_{Nd} values ~1.4‰ and −13.5, respectively, whereas glacial AABW $\delta^{13}C$ is more depleted (−0.5‰) and ε_{Nd} more radiogenic (−5.5) than its modern counterpart (0.4‰, −8.5).

The blue curves show the values expected for conservative mixing between these end-members for each time slice; those points falling along this mixing line have seen little input of biological carbon. During the LGM, data points lying close to the mixing line come from cores shallower than 3,000 m. Most of the glacial data points from cores located below 3,000 m sit well below the mixing curve which we interpret as being caused by the addition of respired organic matter with a low $\delta^{13}C$ (usually ~ −20‰)[41]. It is important to note that these cores represent locations within both northern- and southern- sourced glacial deep water, so this signal was not advected from either

source but was acquired by biological processes along the advection pathway; this highlights the shortcomings of using $\delta^{13}C$ in isolation as a proxy for water mass mixing. The lower than expected $\delta^{13}C$ values could also in part be due to the use of mixed *Cibicidoides* species for some of the benthic foraminiferal $\delta^{13}C$ measurements. The variable depth habitats of different *Cibicidoides* species could lead to offsets of the measured foraminiferal calcite $\delta^{13}C$ from bottom water $\delta^{13}C$ (ref. 42). The inference of organic matter remineralization being the dominant cause of the offset, however, is supported by a recent study that modelled the glacial Atlantic and predicted a biological regenerative imprint in the glacial deep Atlantic $\delta^{13}C$ (ref. 8). The same study calculated that, after allowing for this remineralisation of organic matter, the glacial deep North Atlantic was ventilated by 50–80% NADW, which compares well with the ε_{Nd} derived values of 55–80% NADW produced in this work (Fig. 4b).

The accumulation of respired organic carbon in the deep Atlantic during the LGM could be due to higher surface productivity and thus export of organic carbon to the deep ocean under glacial climate conditions. Although glacial productivity reconstructions in the northwestern Atlantic are sparse, nearby regions show elevated export production during the LGM relative to the Holocene[43]. Higher glacial surface productivity, however, cannot explain the depth dependence of the $\delta^{13}C$ offset in the LGM (Fig. 6b), nor can it explain the chemocline seen at ~2,500 m in nutrient proxy reconstructions[3,4]. Thus it seems likely that the greater amount of respired organic matter in the deep Atlantic during the LGM must have also been at least partially due to a longer residence time of seawater in the glacial deep Atlantic than in the modern Atlantic. This conclusion is supported by a modelling study of a $^{231}Pa/^{230}Th$ data compilation which concluded that the glacial Atlantic had rapid overturning in the shallow cell but slower overturning at depth[44].

Our findings are summarized in hypothetical overturning schematics for the Atlantic Ocean during glacials and interglacials in Fig. 7. In the glacial scenario (Fig. 7b) there are two distinct northern-sourced water masses, separated by density differences. The glacial northern-sourced intermediate depth water mass was

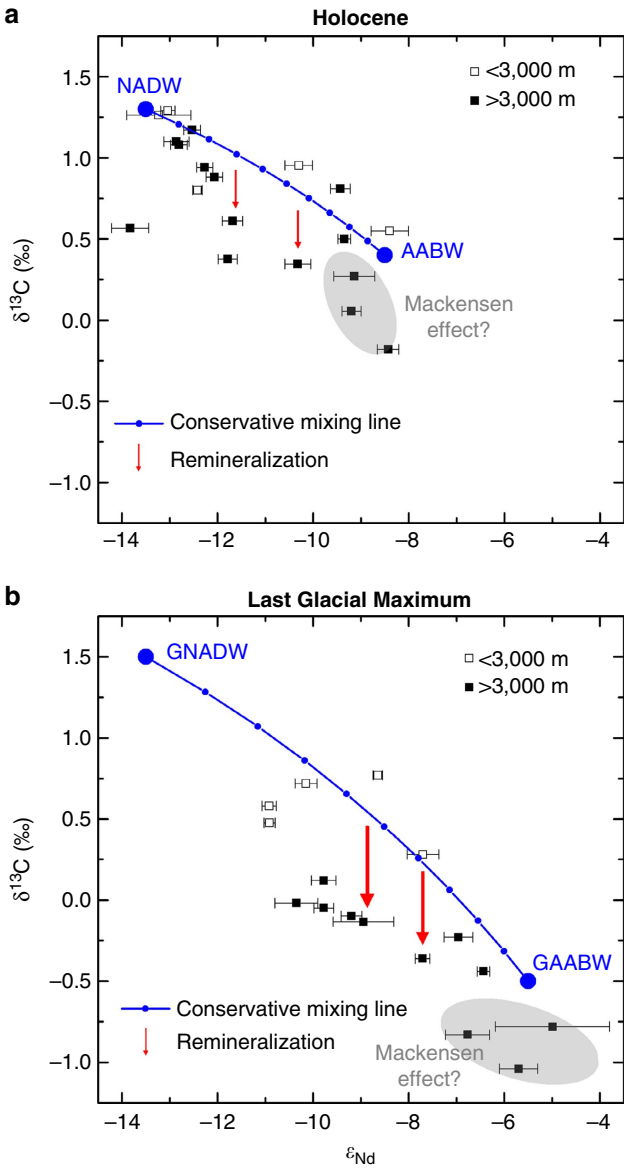

Figure 6 | Cross plots of Atlantic benthic foraminiferal $\delta^{13}C$ against foraminiferal ε_{Nd}. Cross plots of benthic foraminiferal $\delta^{13}C$ against foraminiferal ε_{Nd} for the deep Atlantic Ocean during the (**a**) Holocene and the (**b**) LGM. Water mass end-members labelled are NADW, AABW, GNADW and GAABW. The blue curve shows the values expected for conservative mixing between these water masses in the corresponding cross plot. Offsets from this line are attributed to either the remineralization of organic matter (red arrows) or a possible Mackensen Effect (shaded grey regions)[40]. Details of the data used are given in Supplementary Table 7, and how end-member values were assigned in Supplementary Note 1 and Supplementary Table 8. Error bars show the 2σ external error of the ε_{Nd} measurements.

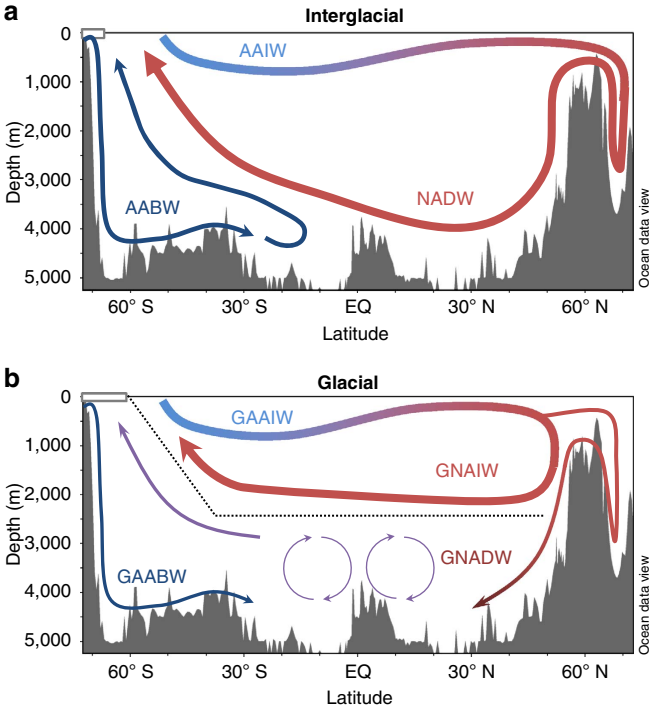

Figure 7 | Interglacial and Glacial Atlantic overturning schematics. Schematics of the structure of Atlantic Meridional Overturning Circulation during (**a**) interglacial and (**b**) glacial periods assuming the Holocene and LGM are typical of each. Water masses depicted are Antarctic Intermediate Water (AAIW), NADW and AABW and their glacial counterparts as well as GNAIW. Thin arrows associated with GNADW and GAABW in the glacial schematic represent the inferred lower flux of these water masses during glacial periods relative to interglacials. The dotted black line in the glacial schematic shows the location of the chemocline in nutrient proxy reconstructions at the interface between the two overturning cells. Figure partly created using Ocean Data View software[22].

likely formed by convection south of Iceland[45] and is inferred to have overturned rapidly[44]. The deep Atlantic cell is surmised to have overturned more slowly and may have been supplied by NADW formed in the Nordic Seas during seasonal ice-free periods coming over the Greenland-Scotland Ridge[46]. Brine rejection from sea ice may also have contributed to this process[47]. A lower flux of GNADW during the LGM than NADW in the Holocene in to the deep North Atlantic would then explain how AABW was able to penetrate much further north during the LGM (Fig. 4b) than in the modern Atlantic Ocean where it has little influence north of the equator (Fig. 4a). In contrast, the deep South Atlantic shows less of a change in water mass mixing proportions between the LGM and the Holocene (Fig. 4) because it is dominated by southern-sourced waters in both climate states (Fig. 7).

Many modelling studies and hypothesized glacial overturning schemes invoke GNAIW being incorporated into deep waters elsewhere in the glacial ocean to ventilate the deep ocean with low-preformed nutrient concentration water[10,13,48]. Here, we have presented evidence that instead the deep Atlantic was ventilated directly from the North Atlantic resolving the difficulty in reconciling glacial CO_2 drawdown with the observed proxy data. Another important prediction of our work is that switching from the glacial to interglacial mode of North Atlantic circulation (Fig. 7) would flush respired organic carbon from the deep Atlantic and would therefore be expected to raise atmospheric CO_2 without invoking changes in nutrient utilization in the high latitude Southern Ocean[13]. Although a full carbon cycle model would be required to quantify this effect, the resumption of strong NADW production at the start of the Bølling-Allerød inferred from ε_{Nd} and $^{231}Pa/^{230}Th$ records, coincides with a $\sim$12 p.p.m. increase in atmospheric CO_2 (Supplementary Fig. 3)[12,18,49]. This increase likely reflects the flushing of respired carbon from the deep Atlantic by strong NADW production during the deglaciation[50].

Methods

Site selection. ε_{Nd} measurements were made on uncleaned planktic foraminifera from Holocene and LGM samples of cores from throughout the western Atlantic basin or selected regions within the eastern Atlantic (Fig. 2d); all core names and locations are listed in Supplementary Table 1 and plotted in Supplementary Fig. 1. Eastern Atlantic cores were limited to sites south of the Walvis Ridge or sites on bathymetric rises above the sill depth of the Mid-Atlantic Ridge (3,750 m)[51]. This selection was based on the criteria outlined by Curry and Oppo[4], and was intended to avoid the regions of the eastern Atlantic which are ventilated through fracture zones in the Mid-Atlantic Ridge and thus do not display the same latitudinal water mass mixing gradient as the western Atlantic[52]. Cores north of 45° N were excluded as they have been shown to be susceptible to the influence of volcanic ash and IRD in the North Atlantic[19,53].

Age controls. Age controls for cores used in this work range from planktic or benthic foraminiferal $\delta^{18}O$ records to radiocarbon dates (Supplementary Table 1) and came from published age models, with the exception of the Ceara Rise cores. The radiocarbon-based age models developed in this work for the latter cores, ODP 925E, ODP 928B and ODP 929B, are presented in Supplementary Table 6. For all cores, depths which were assigned calendar ages between 23 and 18 ka were included in the LGM reconstruction.

Sample preparation. Samples were prepared for analysis following the methods of Roberts *et al.*[18] and references therein. In short, where possible, $\sim$80 mg of mixed planktic foraminifera were picked from the coarse fraction (>63 μm) for neodymium isotope measurements. After picking, foraminifera tests were broken open between two glass plates, rinsed, sonicated and any clays removed. The samples were then dissolved in 1 mol l^{-1} reagent grade acetic acid. The REEs were extracted from the dissolved sample using Eichrom TRUspec resin in 100 ml Teflon columns. Neodymium was then separated from the other rare earth elements using Eichrom LNspec resin on volumetrically calibrated Teflon columns.

Neodymium isotopic measurements. Neodymium isotopes were analysed using the Nu Plasma HR or Neptune Plus multi-collector inductively coupled plasma mass spectrometers at the University of Cambridge. $^{146}Nd/^{144}Nd$ was normalized to 0.7219 and samples were bracketed with a concentration-matched solution of reference standard JNdi-1, the measured composition of which varied between runs but was corrected to the accepted value of $^{143}Nd/^{144}Nd = 0.512115$ (ref. 54). The ε_{Nd} of each sample is reported with the external error (2σ) of the bracketing standards from the corresponding measurement session, unless the internal error was larger than the external error, in which case the combined internal and external error (2σ) is reported.

Eight complete procedural blanks for the process from foraminiferal dissolution through to column chemistry were run on a TIMS Sector 54 at the University of Cambridge using a ^{150}Nd spike. For the typical sample, of at least 15 ng, the average blank of 66 pg of neodymium is $<$0.5% of the total neodymium.

Benthic foraminiferal stable isotopes. Benthic foraminifera (mixed *Cibicidoides* species; between 3 and 7 tests) were picked for stable isotope analysis from the coarse fraction (>125 μm) of samples without published $\delta^{13}C$ data. Samples were analysed by the Godwin Laboratory at the University of Cambridge using either a Micromass Multicarb Sample Preparation System attached to a VG SIRA or a Thermo Kiel device attached to a Thermo MAT253 Mass Spectrometer in dual inlet mode. Isotopic ratios are presented relative to standard Vienna PeeDee Belemnite; external precision was ± 0.06‰ for $\delta^{13}C$.

Data availability. The data reported in this paper are listed in the Supplementary Information and archived in Pangaea (https://doi.pangaea.de/10.1594/PANGAEA.859580).

References

1. Broecker, W. S. Glacial to interglacial changes in ocean chemistry. *Prog. Oceanogr.* **11,** 151–197 (1982).
2. Denton, G. H. *et al.* The last glacial termination. *Science* **328,** 1652–1656 (2010).
3. Lynch-Stieglitz, J. *et al.* Atlantic meridional overturning circulation during the Last Glacial Maximum. *Science* **316,** 66–69 (2007).
4. Curry, W. B. & Oppo, D. W. Glacial water mass geometry and the distribution of $\delta^{13}C$ of ΣCO_2 in the western Atlantic Ocean. *Paleoceanography* **20,** PA1017 (2005).
5. Marchal, O. & Curry, W. B. On the abyssal circulation in the glacial Atlantic. *J. Phys. Oceanogr.* **38,** 2014–2037 (2008).
6. Ferrari, R. *et al.* Antarctic sea ice control on ocean circulation in present and glacial climates. *Proc. Natl Acad. Sci. USA* **111,** 8753–8758 (2014).
7. Negre, C. *et al.* Reversed flow of Atlantic deep water during the Last Glacial Maximum. *Nature* **468,** 84–88 (2010).
8. Gebbie, G. How much did Glacial North Atlantic Water shoal? *Paleoceanography* **29,** 190–209 (2014).
9. Weber, S. L. *et al.* The modern and glacial overturning circulation in the Atlantic ocean in PMIP coupled model simulations. *Clim. Past* **3,** 51–64 (2007).
10. Sigman, D. M., Hain, M. P. & Haug, G. H. The polar ocean and glacial cycles in atmospheric CO_2 concentration. *Nature* **466,** 47–55 (2010).
11. Marinov, I. *et al.* Impact of oceanic circulation on biological carbon storage in the ocean and atmospheric pCO2. *Global Biogeochem. Cycles* **22,** GB3007 (2008).
12. Marcott, S. A. *et al.* Centennial-scale changes in the global carbon cycle during the last deglaciation. *Nature* **514,** 616–619 (2014).
13. Hain, M. P., Sigman, D. M. & Haug, G. H. Carbon dioxide effects of Antarctic stratification, North Atlantic Intermediate Water formation, and subantarctic nutrient drawdown during the last ice age: Diagnosis and synthesis in a geochemical box model. *Global Biogeochem. Cycles* **24,** GB4023 (2010).
14. Frank, M. Radiogenic isotopes: tracers of past ocean circulation and erosional input. *Rev. Geophys.* **40,** doi:10.1029/2000RG000094 (2002).
15. Piepgras, D. J. & Wasserburg, G. J. Rare earth element transport in the western North Atlantic inferred from Nd isotopic observations. *Geochim. Cosmochim. Acta* **51,** 1257–1271 (1987).
16. Stichel, T., Frank, M., Rickli, J. & Haley, B. A. The hafnium and neodymium isotope composition of seawater in the Atlantic sector of the Southern Ocean. *Earth Planet. Sci. Lett.* **317–318,** 282–294 (2012).
17. Amakawa, H., Sasaki, K. & Ebihara, M. Nd isotopic composition in the central North Pacific. *Geochim. Cosmochim. Acta* **73,** 4705–4719 (2009).
18. Roberts, N. L., Piotrowski, A. M., McManus, J. F. & Keigwin, L. D. Synchronous deglacial overturning and water mass source changes. *Science* **327,** 75–78 (2010).
19. Elmore, A. C., Piotrowski, A. M., Wright, J. D. & Scrivner, A. E. Testing the extraction of past seawater Nd isotopic composition from North Atlantic deep sea sediments and foraminifera. *Geochem. Geophys. Geosyst.* **12,** Q09008 (2011).

20. Wilson, D. J., Piotrowski, A. M., Galy, A. & Clegg, J. A. Reactivity of neodymium carriers in deep sea sediments: implications for boundary exchange and paleoceanography. *Geochim. Cosmochim. Acta* **109,** 197–221 (2013).
21. Foster, G. L., Vance, D. & Prytulak, J. No change in the neodymium isotope composition of deep water exported from the North Atlantic on glacial-interglacial time scales. *Geology* **35,** 37–40 (2007).
22. Schlitzer, R. Ocean Data View. http://odv.awi.de (2016).
23. Blanckenburg, F. V. Tracing past ocean circulation? *Science* **286,** 1862b–1863b (1999).
24. Rutberg, R. L., Hemming, S. R. & Goldstein, S. L. Reduced North Atlantic Deep Water flux to the glacial Southern Ocean inferred from neodymium isotope ratios. *Nature* **405,** 935–938 (2000).
25. Wei, R., Abouchami, W., Zahn, R. & Masque, P. Deep circulation changes in the South Atlantic since the Last Glacial Maximum from Nd isotope and multi-proxy records. *Earth Planet. Sci. Lett.* **434,** 18–29 (2016).
26. Piotrowski, A. M. *et al.* Reconstructing deglacial North and South Atlantic deep water sourcing using foraminiferal Nd isotopes. *Earth Planet. Sci. Lett.* **357–358,** 289–297 (2012).
27. Wilson, D. J., Piotrowski, A. M., Galy, A. & Banakar, V. K. Interhemispheric controls on deep ocean circulation and carbon chemistry during the last two glacial cycles. *Paleoceanography* **30,** PA2707 (2015).
28. Noble, T. L., Piotrowski, A. M. & McCave, I. N. Neodymium isotopic composition of intermediate and deep waters in the glacial southwest Pacific. *Earth Planet. Sci. Lett.* **384,** 27–36 (2013).
29. Völker, C. & Köhler, P. Responses of ocean circulation and carbon cycle to changes in the position of the Southern Hemisphere westerlies at Last Glacial Maximum. *Paleoceanography* **28,** 726–739 (2013).
30. Orsi, A. H., Whitworth, T. & Nowlin, W. D. On the meridional extent and fronts of the Antarctic Circumpolar Current. *Deep Sea Res. Part I Oceanogr. Res. Pap.* **42,** 641–673 (1995).
31. Pena, L. D. & Goldstein, S. L. Thermohaline circulation crisis and impacts during the mid-Pleistocene transition. *Science* **345,** 318–322 (2014).
32. Skinner, L. C. *et al.* North Atlantic versus Southern Ocean contributions to a deglacial surge in deep ocean ventilation. *Geology* **41,** 667–670 (2013).
33. Böhm, E. *et al.* Strong and deep Atlantic meridional overturning circulation during the last glacial cycle. *Nature* **517,** 73–76 (2015).
34. Elderfield, H., Whitfield, M., Burton, J. D., Bacon, M. P. & Liss, P. S. The oceanic chemistry of the rare-earth elements [and Discussion]. *Philos. Trans. R. Soc. A Math. Phys. Eng. Sci.* **325,** 105–126 (1988).
35. Crocket, K. C., Vance, D., Gutjahr, M., Foster, G. L. & Richards, D. A. Persistent Nordic deep-water overflow to the glacial North Atlantic. *Geology* **39,** 515–518 (2011).
36. Rempfer, J., Stocker, T. F., Joos, F. & Dutay, J.-C. Sensitivity of Nd isotopic composition in seawater to changes in Nd sources and paleoceanographic implications. *J. Geophys. Res.* **117,** C12010 (2012).
37. Skinner, L. C., Waelbroeck, C., Scrivner, A. E. & Fallon, S. J. Radiocarbon evidence for alternating northern and southern sources of ventilation of the deep Atlantic carbon pool during the last deglaciation. *Proc. Natl. Acad. Sci. USA* **111,** 5480–5484 (2014).
38. Yu, J., Elderfield, H. & Piotrowski, A. M. Seawater carbonate ion-$\delta^{13}C$ systematics and application to glacial–interglacial North Atlantic ocean circulation. *Earth Planet. Sci. Lett.* **271,** 209–220 (2008).
39. Yu, J. *et al.* Deep South Atlantic carbonate chemistry and increased interocean deep water exchange during last deglaciation. *Quat. Sci. Rev.* **90,** 80–89 (2014).
40. Mackensen, A., Hubberten, H., Bickert, T. & Ftitterer, D. K. The $\delta^{13}C$ in benthic foraminifera tests of *Fontbotia wuellerstorfi* (Schwager) relative to the $\delta^{13}C$ of dissolved inorganic carbon in Southern Ocean deep water: implications for glacial ocean circulation models. *Paleoceanography* **8,** 587–610 (1993).
41. Kroopnick, P. The distribution of ^{13}C of ΣCO_2 in the world oceans. *Deep. Sea Res. Part A Oceanogr. Res. Pap.* **32,** 57–84 (1985).
42. Hodell, D. A., Venz, K. A., Charles, C. D. & Ninnemann, U. S. Pleistocene vertical carbon isotope and carbonate gradients in the South Atlantic sector of the Southern Ocean. Geochemistry. *Geophys. Geosyst.* **4,** 1–19 (2003).
43. Kohfeld, K. E., Le Quéré, C., Le, Harrison, S. P. & Anderson, R. F. Role of Marine Biology in Glacial-Interglacial CO_2 Cycles. *Science* **308,** 74–78 (2005).
44. Lippold, J. *et al.* Strength and geometry of the glacial Atlantic Meridional Overturning Circulation. *Nat. Geosci.* **5,** 813–816 (2012).
45. Labeyrie, L. D. *et al.* Changes in the vertical structure of the North Atlantic Ocean between glacial and modern times. *Quat. Sci. Rev.* **11,** 401–413 (1992).
46. Millo, C., Sarnthein, M., Voelker, A. & Erlenkeuser, H. Variability of the Denmark Strait Overflow during the Last Glacial Maximum. *Boreas* **35,** 50–60 (2006).
47. Dokken, T. & Jansen, E. Rapid changes in the mechanism of ocean convection during the last glacial period. *Nature* **401,** 458–461 (1999).
48. Kwon, E. Y. *et al.* North Atlantic ventilation of 'southern-sourced' deep water in the glacial ocean. *Paleoceanography* **27,** 1–12 (2012).
49. McManus, J. F., Francois, R., Gherardi, J.-M., Keigwin, L. D. & Brown-Leger, S. Collapse and rapid resumption of Atlantic meridional circulation linked to deglacial climate changes. *Nature* **428,** 834–837 (2004).
50. Chen, A. T. *et al.* Synchronous centennial abrupt events in the ocean and atmosphere during the last deglaciation. *Science* **349,** 1537–1542 (2015).
51. Metcalf, W. G., Heezen, B. C. & Stalcup, M. C. The sill depth of the Mid-Atlantic Ridge in the equatorial region. *Deep Sea Res. Oceanogr. Abstr.* **11,** 1–10 (1964).
52. McCartney, M. S., Bennett, S. L. & Woodgate-Jones, M. E. Eastward flow through the Mid-Atlantic Ridge at 11° N and its influence on the abyss of the eastern basin. *J. Phys. Oceanogr.* **21,** 1089–1121 (1991).
53. Roberts, N. L. & Piotrowski, A. M. Radiogenic Nd isotope labeling of the northern NE Atlantic during MIS 2. *Earth Planet. Sci. Lett.* **423,** 125–133 (2015).
54. Tanaka, T. *et al.* JNdi-1: a neodymium isotopic reference in consistency with LaJolla neodymium. *Chem. Geol.* **168,** 279–281 (2000).
55. Jeandel, C. Concentration and isotopic composition of Nd in the South Atlantic Ocean. *Earth Planet. Sci. Lett.* **117,** 581–591 (1993).
56. Huang, K.-F., Oppo, D. W. & Curry, W. B. Decreased influence of Antarctic intermediate water in the tropical Atlantic during North Atlantic cold events. *Earth Planet. Sci. Lett.* **389,** 200–208 (2014).
57. Jonkers, L. *et al.* Deep circulation changes in the central South Atlantic during the past 145 kyrs reflected in a combined $^{231}Pa/^{230}Th$, Neodymium isotope and benthic $\delta^{13}C$ records. *Earth Planet. Sci. Lett.* **419,** 14–21 (2015).
58. Gutjahr, M., Frank, M., Stirling, C. H., Keigwin, L. D. & Halliday, A. N. Tracing the Nd isotope evolution of North Atlantic Deep and Intermediate Waters in the western North Atlantic since the Last Glacial Maximum from Blake Ridge sediments. *Earth Planet. Sci. Lett.* **266,** 61–77 (2008).
59. Lang, D. C. *et al.* Incursions of southern-sourced water into the deep North Atlantic during late Pliocene glacial intensification. *Nat. Geosci.* **9,** 375–379 (2016).

Acknowledgements

Sample material was provided by the Godwin Laboratory for Paleoclimate Research at the University of Cambridge, the International Ocean Discovery Program the GeoB Core Repository at the MARUM—Center for Marine Environmental Sciences, University of Bremen and Petrobras. We thank Jo Kerr and Aurora Elmore for providing additional samples. We thank Thiago Pereira dos Santos for providing the unpublished age model data for GL1090; we thank Jo Clegg and Vicky Rennie for technical support and Natalie Roberts for helpful discussions. Radiocarbon analyses were supported by NERC radiocarbon grant 1752.1013 and Nd isotope analyses by NERC grants NERC NE/K005235/1 and NERC NE/F006047/1 to A.M.P. J.N.W.H. was supported by a Rutherford Memorial Scholarship. S.M. was supported through the DFG Research Center/Cluster of Excellence 'The Ocean in the Earth System'. C.M.C. acknowledges financial support from FAPESP (grant 2012/17517-3).

Author contributions

J.N.W.H. and A.M.P. designed the study, J.N.W.H. performed the work, and J.N.W.H. and A.M.P. wrote the manuscript with contributions from all other authors. T.L.N. provided unpublished data from ODP 1088; S.M., C.M.C. and G.B. provided sample material and unpublished data.

Additional information

Supplementary Information accompanies this paper at http://www.nature.com/naturecommunications

Competing financial interests: The authors declare no competing financial interests.

Reprints and permission information is available online at http://npg.nature.com/reprintsandpermissions/

How to cite this article: Howe, J. N. W. *et al.* North Atlantic Deep Water Production during the Last Glacial Maximum. *Nat. Commun.* 7:11765 doi: 10.1038/ncomms11765 (2016).

nature COMMUNICATIONS

ARTICLE

Received 7 Dec 2015 | Accepted 19 May 2016 | Published 27 Jun 2016

DOI: 10.1038/ncomms11998 OPEN

Radiocarbon evidence for enhanced respired carbon storage in the Atlantic at the Last Glacial Maximum

E. Freeman[1], L.C. Skinner[1], C. Waelbroeck[2] & D. Hodell[1]

The influence of ocean circulation changes on atmospheric CO_2 hinges primarily on the ability to alter the ocean interior's respired nutrient inventory. Here we investigate the Atlantic overturning circulation at the Last Glacial Maximum and its impact on respired carbon storage using radiocarbon and stable carbon isotope data from the Brazil and Iberian Margins. The data demonstrate the existence of a shallow well-ventilated northern-sourced cell overlying a poorly ventilated, predominantly southern-sourced cell at the Last Glacial Maximum. We also find that organic carbon remineralization rates in the deep Atlantic remained broadly similar to modern, but that ventilation ages in the southern-sourced overturning cell were significantly increased. Respired carbon storage in the deep Atlantic was therefore enhanced during the last glacial period, primarily due to an increase in the residence time of carbon in the deep ocean, rather than an increase in biological carbon export.

[1] Godwin Laboratory for Palaeoclimate Research, Department of Earth Sciences, University of Cambridge, Cambridge CB2 3EQ, UK. [2] LSCE/IPSL, Laboratoire CNRS-CEA-UVSQ, Domaine du CNRS, bât 12 91198 Gif-sur-Yvette, France. Correspondence and requests for materials should be addressed to E.F. (email: ef276@cam.ac.uk).

Numerous proxies suggest that ocean circulation at the Last Glacial Maximum (LGM) was different from modern, especially in the Atlantic Ocean[1–4]. Despite this, a consensus has yet to emerge on the LGM ocean circulation[5], primarily because of limitations associated with the various proxies, as well as a paucity of data. In agreement with stable oxygen isotope data[6], $\delta^{13}C$ (stable carbon isotopic ratio) and Cd/Ca data suggest that North Atlantic Deep Water (NADW) shoaled by up to 1,000 m during the LGM relative to today[3,4,7]. However, the combination of conservative and non-conservative impacts on nutrient proxies has permitted alternative interpretations, such as greater nutrient accumulation along the flow path[8] (because of greater export production or longer transit times), or variable contributions from northern- and southern-sourced waters between 2 and 4 km water depth[9] (without a complete elimination of NADW in the deep Atlantic). Although $^{231}Pa/^{230}Th$ has been used to reconstruct past rates of overturning circulation[10,11], its interpretation presents difficulties, as it represents an integrated flow speed across the water column and may be affected by scavenging[12].

Additional proxy data are therefore needed to reconstruct the pattern and rate of ocean circulation at the LGM, and to assess its impact on the marine carbon cycle. Radiocarbon-based ventilation ages could prove particularly useful in this regard as they provide an indication of the mean timescale for carbon exchange between the ocean and the atmosphere, including the effects of air–sea gas (and isotope) exchange in the regions of origin of a given parcel of water, and the mean time elapsed since that water was in the mixed layer. Furthermore, by combining ventilation ages with indicators of respired carbon accumulation, such as stable carbon isotopes, changes in the efficiency of the biological carbon pump can be estimated. This is not possible using reconstructions of flow rates or respired/total nutrient levels alone, as the efficiency of the biological carbon pump is controlled by both the export productivity (that is, the flux of carbon into the deep ocean) and the 'leakage' of this carbon out of the deep ocean (via all the processes that contribute to mass transfer from the deep ocean interior to the surface ocean mixed layer where air–sea exchange occurs).

Here we investigate the Atlantic Ocean overturning circulation at the LGM using both radiocarbon and stable carbon isotopes. We find a shallow well-ventilated northern-sourced cell overlying a poorly ventilated, predominantly southern-sourced cell. Furthermore, we find that the storage of respired carbon in the deep Atlantic Ocean was enhanced because of a long residence time, with a constant flux of respired carbon to the deep Atlantic.

Results

Radiocarbon and stable carbon isotopes. Here we present new radiocarbon-based ventilation ages along with stable carbon isotopes from 1,000 to 3,500 m on the Brazil Margin and from 1,100 to 4,700 m on the Iberian Margin (Supplementary Table 1). Ventilation ages are based on benthic-planktonic (B-P) radiocarbon age offsets, to which the estimated surface reservoir age is added to provide an estimate of the deep ocean versus atmospheric radiocarbon age offset (B-Atm). Given the proximity of cores in each of our study regions, surface reservoir ages are expected to be very similar for all cores in each transect. Therefore, despite some uncertainty in the surface reservoir ages, vertical gradients in ventilation ages within each transect will remain accurate.

Radiocarbon-based ventilation ages provide an indication of the extent of isotopic disequilibrium between the marine- and atmospheric carbon reservoirs. More radiocarbon-depleted waters (indicated by higher radiocarbon ventilation ages) will reflect less efficient radiocarbon (and therefore CO_2) exchange between the ocean interior and the atmosphere on average, and therefore a longer carbon sequestration time in the ocean interior. For continuous export of biologically fixed carbon to the ocean interior, a greater radiocarbon ventilation age and a longer carbon sequestration time (that is, relative to the atmosphere) should in turn reflect enhanced accumulation of respired carbon in the ocean interior and a more efficient (since less 'leaky') soft-tissue carbon pump[13].

Ventilation of the Brazil Margin. On the Brazil Margin, the radiocarbon ventilation age-depth profile for the LGM is significantly different from that of the modern ocean (Fig. 1). Although the shallowest core (1,000 m), has a similar ventilation age to that of the modern ocean, the deeper cores have considerably higher ventilation ages, with the deepest core being offset from the surface ocean by up to 1,700 years, compared with just 400 years today.

Stable carbon isotopes also had a distinctly different profile at the LGM compared with the modern. $\delta^{13}C$ shows a significant decrease with depth, ranging from $\sim$1.1‰ at 1,000 m to $\sim$0.2‰ in the deep ocean. The steepest gradient (~ -0.5‰/1,000 m) is seen between 2,300 and 3,550 m, whereas in the modern ocean the gradient is $<$0.02‰/1,000 m between these depths.

Ventilation of the Iberian Margin. The Iberian Margin also shows a very different ventilation age depth-profile at the LGM compared with the modern ocean (Fig. 1). Although the intermediate ocean ($<$2,100 m) was well ventilated, the deep ocean was poorly ventilated, with B-P age offsets more than 1,000 years greater than in the modern ocean. The shallowest core (1,127 m) has a negative B-P age offset suggesting that the surface was more poorly ventilated than the intermediate ocean (likely influenced by Mediterranean Outflow Water[14]). Beneath this, the B-P age offset increases with depth in the water column. A relatively steep gradient ($\sim$950 years/1,000 m) is seen for the upper 2,600 m, with a smaller increase in B-P age offset with depth below ($\sim$200 years/1,000 m). A similar profile is also seen in $\delta^{13}C$ with a steep gradient (~ -0.4‰/1,000 m) between 2 and 3.7 km but with relatively little change (< -0.1‰/1,000 m) with depth below $\sim$3,700 m. The range of $\delta^{13}C$ (0–0.8‰) at the LGM is significantly greater than the range in the modern North Atlantic (1.0–1.1‰) between 2 and 4.7 km. $\delta^{13}C$ at 4.7 km are more than 0.9‰ lower at the LGM than in the modern ocean. However, extremely low $\delta^{13}C$, previously observed in both the deep South Atlantic (< -0.8‰)[15,16] and in the abyssal western North Atlantic (-0.3 to -0.5‰)[17,18], are not observed in any of the Iberian Margin cores.

Discussion

We combined our new ventilation ages with available published data in order to tentatively reconstruct the distribution of radiocarbon in the Atlantic Ocean during the LGM[18–25] (Fig. 2 and Supplementary Table 2). These radiocarbon-based ventilation ages show that, regardless of the uncertainties in LGM surface reservoir ages, the entire deep Atlantic Ocean ($>$2 km) was less ventilated during the LGM than the modern ocean (Fig. 3). Today, the deep North Atlantic is well ventilated by newly formed NADW, whereas the deep South Atlantic is primarily influenced by southern-sourced waters (Lower Circumpolar Deep Water, LCDW, and Antarctic Bottom Water, AABW), which have greater ventilation ages because of reduced air–sea gas exchange in the AABW formation regions[26] and because of mixing and entrainment of 'pre-aged' circumpolar deep water into AABW[27]. During the LGM this North–South

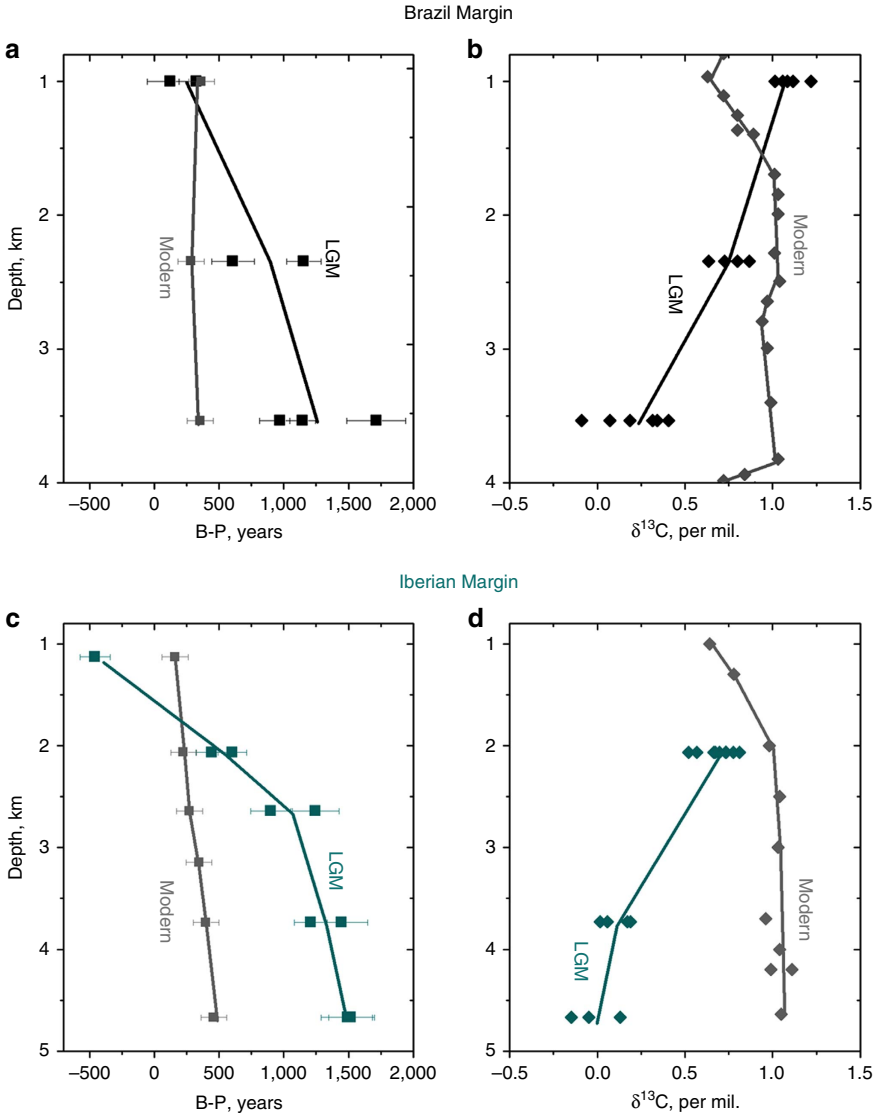

Figure 1 | LGM depth profiles for the Brazil Margin and the Iberian Margin. The benthic-planktonic radiocarbon age offset (B-P; **a**, **c**) and the stable carbon isotopic ratio, $\delta^{13}C$ (**b**, **d**). Modern B-P values (calculated by subtracting the modern surface reservoir age from the bottom water ventilation age) are show in grey (GLODAP[38]). Modern $\delta^{13}C$ of DIC is also shown in grey (GEOSECS[38]). Data are given in Supplementary Table 3.

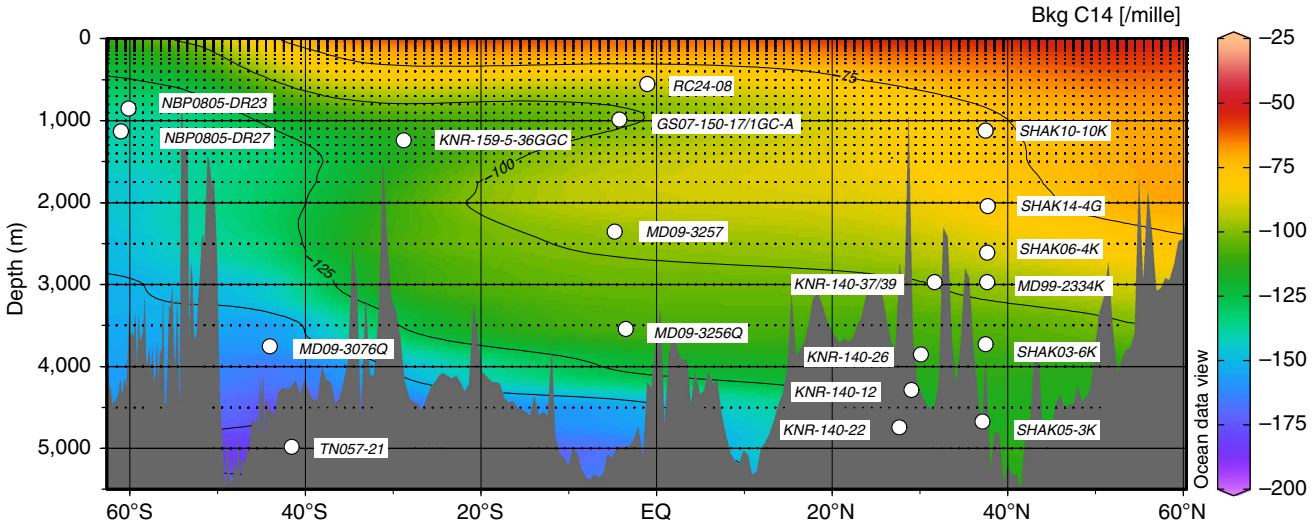

Figure 2 | Map of core locations. Map showing core/dredge locations with modern background $\Delta^{14}C$ (GLODAP[38]), using Ocean Data View[71].

ventilation age gradient in the deep Atlantic was significantly reduced or even eradicated (in the abyss), suggesting a distinctly different circulation must have prevailed (Figs 3 and 4). Based on the apparent northward expansion of poorly ventilated deep waters from the glacial South Atlantic to the deep equatorial and North Atlantic, the LGM circulation appears to have been characterized primarily by a greatly reduced influence of NADW in the deepest Atlantic (>2,000 m). It is notable that abyssal waters in the western North Atlantic and on the northern Brazil Margin had a similar ventilation age to that of the abyssal South Atlantic (Fig. 3). The lack of an increase in ventilation age along the flow path between the South Atlantic and the equatorial and North Atlantic suggests that neither the deep eastern Atlantic nor the deep western Atlantic contained pure southern-sourced waters. A persistent, albeit greatly reduced, northern source of radiocarbon was therefore provided to depths of at least 4.7 km, either via mixing with an overlying well-ventilated water mass or via direct episodic input of dense well-ventilated (for example, overflow) waters.

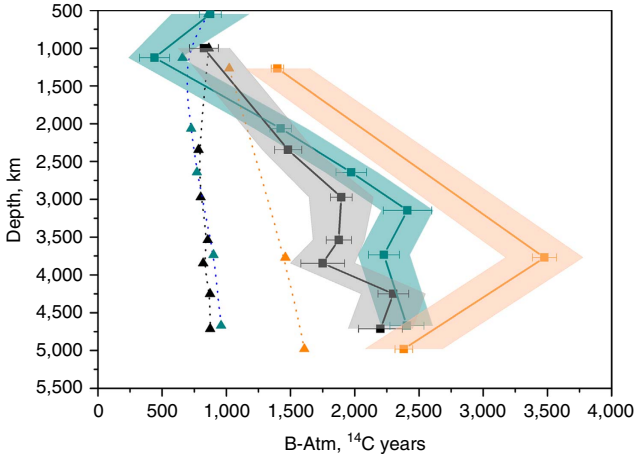

Figure 3 | Atlantic radiocarbon-based ventilation age depth profiles. Triangles: modern ventilation ages (dotted lines). Squares: LGM ventilation ages (solid lines)[18–24,34]. Error bars indicate the analytical error on the radiocarbon measurements. The shaded area represents the uncertainty of the surface reservoir age. Blue, East Atlantic; black, West Atlantic; orange, South Atlantic.

In the modern ocean, radiocarbon-based ventilation ages are well correlated with DIC and anti-correlated with $\delta^{13}C$ owing to the remineralization of organic carbon as waters flow from the North Atlantic to the North Pacific, via the Southern Ocean (Fig. 5). DIC thus increases in the modern ocean by $\sim$115 µmol kg^{-1} (ref. 13), whereas the $\delta^{13}C$ of DIC decreases by $\sim$0.8‰ (Fig. 5), for every 10% decrease in the deep ocean's radiocarbon content relative to the atmosphere (that is, for every $\sim$850 ^{14}Cyr ventilation age increase). A similar gradient in $\delta^{13}C$ versus ventilation age is seen in the North and equatorial Atlantic

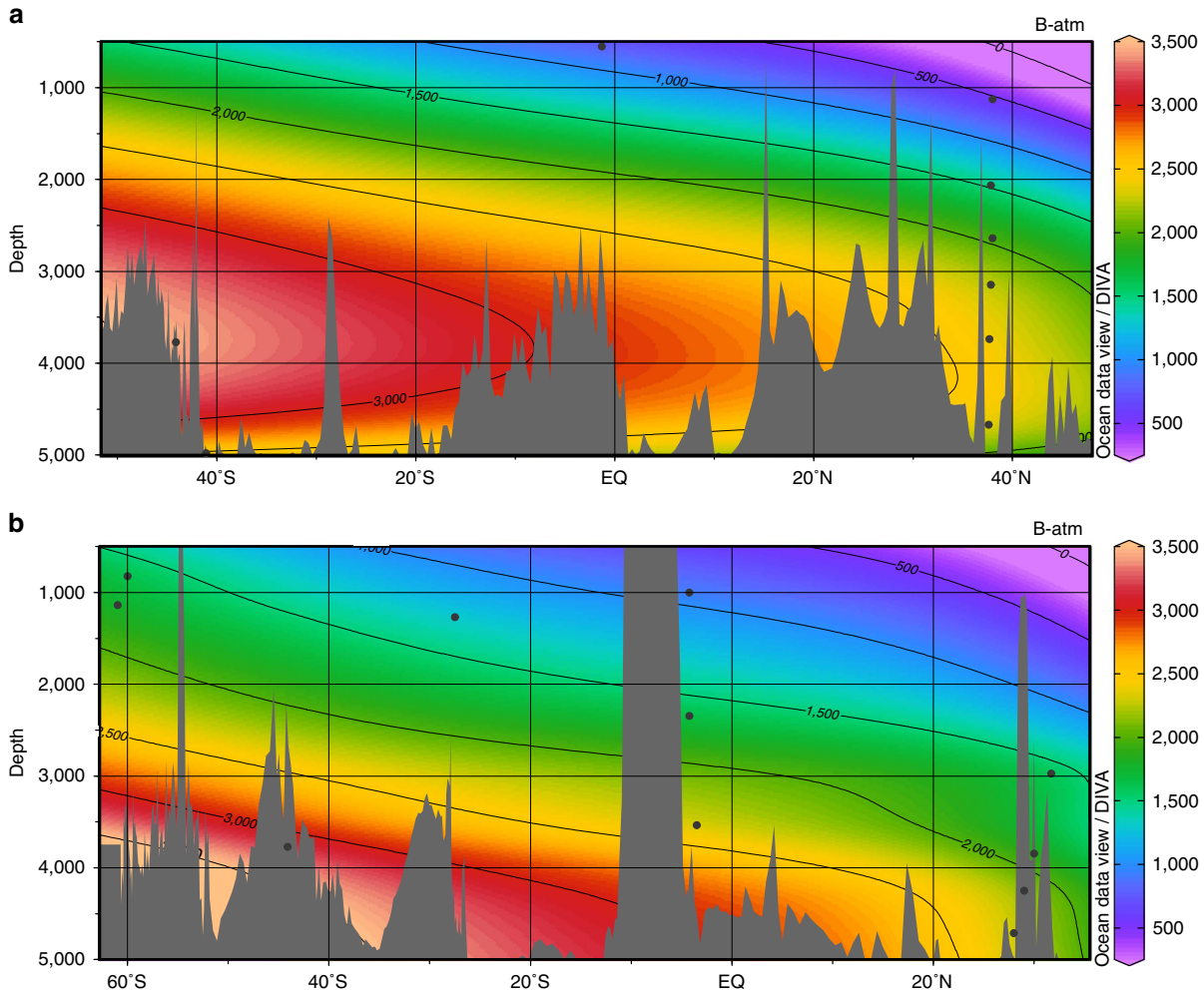

Figure 4 | Atlantic radiocarbon based ventilation ages at the LGM. (**a**) Eastern Atlantic. (**b**) Western Atlantic[18–25,34]. MD07-3076Q (44°S, 14°W, 3770 m) is included in both the eastern and the western profiles as it is located on the Mid-Atlantic Ridge. The dots indicate the position of the cores where ventilation ages have been determined. Gridded in ODV[71] using DIVA gridding with a signal-to-noise ratio of 72. Data are given in Supplementary Table 4.

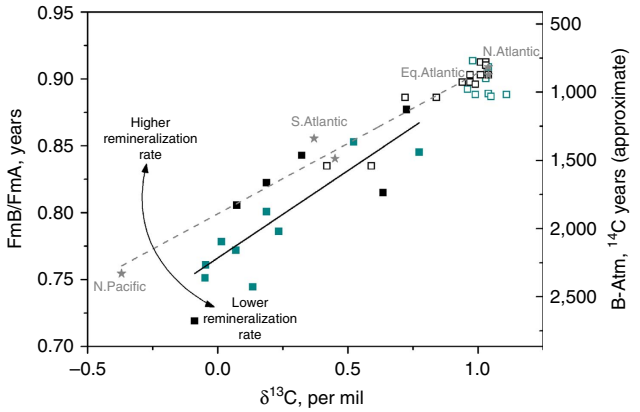

Figure 5 | Crossplot of ventilation age and stable carbon isotopic ratio. Ventilation ages are plotted as FmB/FmA, where FmB/FmA = exp(B-Atm/-8033), and Fm = fraction modern, because B-Atm ages do not mix linearly due to the exponential decay of radiocarbon. Approximate B-Atm values are shown as a guideline only. Modern whole ocean data (~2.5 km water depth; grey stars) is show along with modern data for the entire water column >2 km (open squares) on the Iberian Margin (blue) and Brazil Margin (black). LGM data are shown (filled squares) for the Iberian Margin (blue) and the Brazil Margin (black; Modern data are from GEOSECS and GLODAP[38]). The modern gradient is 0.11 ± 0.01 and the LGM gradient is 0.13 ± 0.02, equivalent to 1.1 ± 0.1‰/kyr and 0.9 ± 0.2‰/kyr in the modern and in the LGM, respectively. For a given rate of remineralization, an increase in residence time (that is, lower FmB/FmA) results in a greater amount of carbon storage.

at the LGM, suggesting that the remineralization rate of organic carbon in the deep Atlantic did not change significantly. On this basis, the LGM rate of DIC increase per year of radiocarbon decay (because of the soft-tissue pump alone) would also be expected to have remained roughly constant, as hypothesized in ref. 13. All else being equal, the ventilation age increase that we observe across the deep Atlantic would therefore imply a significant increase in the respired carbon inventory of the deep ocean at the LGM. This increase was proposed in ref. 8 but later questioned in ref. 9 because of an updated LGM state estimate. Here we not only propose an increase in the remineralized carbon inventory of the deep ocean (based on stable carbon isotope evidence, similar to that advanced previously), but also attribute it to an increase in residence time rather than an increase in biological carbon export rates.

Our results demonstrate a distinct difference in the distribution of radiocarbon in the Atlantic at the LGM relative to today. The deep ocean was more poorly ventilated at all latitudes, whereas the intermediate ocean remained as well ventilated as in the modern ocean. This strongly suggests a shoaling of northern-sourced waters, without a major reduction in their overturning strength, and an expansion of southern-sourced waters at depth. This is in agreement with other proxy reconstructions, which our radiocarbon data help to link more directly to carbon cycle impacts. The concentration of dissolved cadmium inferred from Cd/Ca measured on benthic foraminifera show a clear decrease in the upper ~2.2 km of the water column at the LGM relative to today, with the opposite sense of change in the deep ocean[4] (Supplementary Fig. 1a). This would suggest that high-nutrient waters expanded at depth while low-nutrient northern-sourced waters dominated in the intermediate ocean, consistent with $\delta^{13}C$ data that also show the opposite sense of change above and below ~2.2 km (ref. 4; Supplementary Fig. 1b). In principle, this change in nutrient distributions could have been driven by enhanced export productivity and/or longer ocean interior residence times. As indicated above, our combined radiocarbon and stable isotope data indicate that the latter mechanism was dominant. Our interpretation that this change in circulation was primarily associated with an expansion of southern-sourced waters in the deepest Atlantic is further supported by εNd data, which indicate an increase in southern-sourced waters at depth with an increase in northern-sourced waters above[28] (Supplementary Fig. 1c). $^{231}Pa/^{230}Th$ ratios also display a distinct change of the opposite sign above and below ~2.2 km water depth[10] (Supplementary Fig. 1d). These $^{231}Pa/^{230}Th$ ratios suggest that the North Atlantic overturning circulation cell was just as strong during the LGM as it is today, but that it penetrated to shallower depths. Although this contrasts with many numerical modelling studies that tend to find a slower overturning when NADW shoals[29,30], our ventilation ages also suggest that the upper North Atlantic overturning rate was not reduced so much that it significantly decreased the supply radiocarbon to the intermediate ocean. The radiocarbon data are therefore consistent with the proposal that a significant shoaling of NADW may not necessarily imply a major reduction in the NADW formation/transport rate at the LGM.

However, while our results support the existence at the LGM of a shallow NADW cell overlying an expanded, radiocarbon-depleted AABW below, they also suggest that the deep southern-sourced cell was not completely isolated. In both the eastern and the western North Atlantic, a northern source of relatively radiocarbon-enriched and high $\delta^{13}C$ waters was mixed into the deep cell. This could imply a more complex Atlantic circulation than one characterized by two completely separate overturning cells at the LGM[31], where the northern overturning cell is either strong and deep or weak and shallow.

As in the landmark study of ref. 3, our stable isotope data demonstrate the existence of enhanced gradients in $\delta^{13}C$ between ~2,000 and 3,500 m in the equatorial and North Atlantic. This pattern of $\delta^{13}C$ in the Atlantic has been interpreted primarily to demonstrate a reduction in the proportion of northern-sourced waters with depth, and an increase in the total nutrient content of the deep Atlantic. Our new radiocarbon data demonstrate that this did not primarily reflect an increase in 'preformed' nutrients (that is, nutrients that were advected to the ocean interior, and that would be associated with carbon that was well-equilibrated with the atmosphere[32]), but rather an increase in respired nutrients (and therefore respired carbon). Alternatively, and equivalently for ocean versus atmosphere carbon inventory changes, the radiocarbon data might also indicate an increase in the 'disequilibrium' carbon inventory of the deep Atlantic[33]. However, in this case, a very large decrease in air–sea CO_2 exchange efficiency would need to be invoked in parallel with an increase in preformed nutrients, in order to account for the paired stable carbon isotope (and nutrient) reconstructions. The observed expansion of southern-sourced deep waters at the LGM was therefore very likely associated with an increase in the efficiency of the soft-tissue carbon pump, primarily due to an increase in the residence time of carbon in the deep Atlantic, rather than an increase in biological export productivity (that is, at low/mid-latitudes). Although global data coverage and better constraints on surface reservoir ages are required to assess the precise magnitude of the atmospheric CO_2 drawdown that is implied by the observed ocean circulation changes, our findings support a direct contribution from the Atlantic overturning circulation via its impact on the deep ocean's respired carbon inventory.

Methods

Radiocarbon and stable carbon isotope measurements. Radiocarbon ages were measured on benthic and planktonic foraminifera from a series of cores recovered from the Brazil Margin by the R/V *Marion Dufresne* (MD09-3256Q, MD09-3257)

and the Iberian Margin by the R/V *James Cook* (SHAK03-6K, SHAK05-3K, SHAK06-4K, SHAK10-10K and SHAK14-4G; Fig. 2). Results from these cores are combined with previously published data from the same transect regions (MD99-2334K and GS07-150-17/1GC-A)[22,34]. Core locations are given in Supplementary Table 1. Benthic stable carbon isotopes were also measured in these cores on *Cibicidoides wuellerstorfi*. No stable carbon isotopes were measured for SHAK10-10K because of the lack of any specimens of *Cibicidoides*.

Foraminifera were picked from the >212 μm size fraction and where necessary from the 150–212 μm fraction. Samples of *Globigerinoides ruber* (Brazil Margin) or *Globigerina bulloides* (Iberian Margin) and samples of mixed benthic foraminifera (excluding agglutinated species) were picked and graphitized in the Godwin Radiocarbon Laboratory at the University of Cambridge. Stable carbon isotope measurements were conducted on *Cibicidoides wuellerstorfi* and on DIC at the Godwin Laboratory, Cambridge.

Radiocarbon measurements. Samples were cleaned on a glass plate with deionized water to remove any loose material. Samples were then dried and acidified. The CO_2 produced was converted to graphite using a standard hydrogen/iron catalyst reduction method[35]. AMS-^{14}C dates were obtained for the graphite samples at the ^{14}Chrono Centre, Queens University Belfast. All dates are reported as conventional radiocarbon ages following[36].

Stable carbon isotope measurements on foraminifera. Stable carbon isotope measurements were conducted on *Cibicidoides wuellerstorfi* in the Godwin Laboratory. Each measurement was run on 1–3 individuals with a combined mass of 50–180 μg. The foraminifera were transferred into sample vials, crushed and then dried in an oven at 50 °C. Samples were reacted with orthophosphoric acid (100%) and the CO_2 produced was cryogenically dried and then admitted to the dual inlet mass spectrometer for isotopic analysis by comparison with a reference gas. Each run of 30 samples was accompanied by 10 reference carbonates and 2 control samples. The results are reported with reference to the international standard VPDB and the precision is better than ±0.06‰ for ^{12}C/^{13}C and ±0.08‰ for ^{16}O/^{18}O.

Stable carbon isotope DIC measurements. DIC measurements were made using a Thermo Gas Bench attached to a Delta V Mass Spectrometer. Three or four drops of orthophosphoric acid (100%) were preloaded into a reaction vial, which was capped, sealed and the headspace flushed with Helium gas. Approximately 1.5 ml of sample water was injected into the vial through the butyl rubber septa using a syringe and left to react for 1 h. The sample tubes were transferred to the Gas Bench and CTC CombiPal Autosampler and the resulting CO_2 in the headspace analysed using a Thermo Delta V Mass Spectrometer. A series of standards and reference samples distributed throughout the run were used to calibrate to the international standard VPDB. Results have a reproducibility of better than 0.1 per mille.

Ventilation ages. Here we report ventilation ages as either deep to shallow sub-surface radiocarbon age offsets, based on benthic-planktonic radiocarbon age differences (B-P), or as deep-atmospheric radiocarbon age offsets (B-Atm), which represent the B-P plus the surface reservoir age (that is, the shallow sub-surface versus atmosphere radiocarbon disequilibrium) that applies to the planktonic radiocarbon age. Although B-P offsets provide useful (and very accurate) information regarding vertical radiocarbon gradients at various locations in the ocean, B-Atm estimates are advantageous by virtue of referencing radiocarbon activities throughout the ocean interior relative to a single reference point: the radiocarbon activity of the atmosphere. They also maintain a constant scaling with respect to radiocarbon disequilibria, unlike relative isotopic offset metrics such as Δ^{14}C (ref. 37). When mapped throughout the ocean, B-Atm offsets may thus provide a coherent means of inferring the patterns and rates of ocean-atmosphere CO_2 exchange and transport in the ocean interior[38]. However, the uncertainty associated with LGM surface reservoir age estimates makes the derivation of accurate B-Atm offsets challenging.

Surface reservoir ages at the LGM. To accurately reconstruct the distribution of radiocarbon in the Atlantic Ocean at the LGM, benthic radiocarbon activities must be referenced to a single (atmospheric) reference point. Therefore, we need to not only consider the deep- to surface age differences but also the surface to atmosphere age offsets that apply in each instance (alternatively each benthic radiocarbon date can be directly compared with the contemporary atmospheric radiocarbon age, given independent calendar ages). The planktonic foraminifera used in this study calcify in the upper surface ocean (<100 m deep), but even at these depths the water can be in significant disequilibrium relative to the atmosphere. Today surface reservoir ages range from around 400 to 600 years on the Brazil and Iberian Margins (GLODAP[38]). However, these would have varied in the past due to changes in pCO_2 (affecting air–sea carbon isotope exchange at a given CO_2 solubility), changes in ocean circulation (influencing the mixing/upwelling of 'aged' waters into the surface ocean mixed layer) and, for example, changes in high latitude temperature, salinity and sea-ice cover (affecting CO_2 solubility and gas exchange in sub- mixed-layer source regions). However, determining surface reservoir ages in the past is challenging, and not possible in contexts where independent calendar age or contemporaneous atmospheric radiocarbon age constraints are lacking. The modern surface reservoir age is therefore often used as a best guess, under the tentative assumption that physical conditions affecting radiocarbon exchange and transport have not changed over time[24,39,40].

To accurately determine surface reservoir ages, a calendar age model that is independent of radiocarbon dating and a history of atmospheric radiocarbon variability are required. Although U/Th dating can be used to provide calendar ages for corals[43], chronostratigraphic (including tephrochronological) approaches must be used for sediment cores. In high latitudes, cores can be linked stratigraphically to independently dated ice cores[21,22,41]. However, for low latitude, cores in which chronostratigraphic signals are typically more subdued and synchrony with high-latitude climate changes may be questionable, it is much more difficult to obtain an independent calendar chronostratigraphy. Yet, it is important to note that even at low latitudes, especially in regions with deep mixed layers or upwelling regimes, shallow sub-surface radiocarbon disequilibria are very likely to have changed across the last deglaciation[42,43].

Although it is possible in principle to use model simulations to infer past surface reservoir ages, this approach requires knowledge of past changes in ocean circulation and ocean–atmosphere gas exchange efficiency (for example, because of changes in sea-ice extent or mixed layer depths), which strictly we do not have (indeed, this is typically what we are seeking). Despite this fundamental limitation, efforts have been made to model surface reservoir ages in the past, for example, assuming a constant ocean circulation[44,45]. These studies have shown that at the LGM the pCO_2 difference alone would have caused surface reservoir ages to be around 250 years higher than under modern conditions—a passive response in the ocean that does not reflect the ocean's impact on atmospheric CO_2 but rather the atmosphere's impact on the ocean. Additional changes in the mean exchange rate of CO_2 between the ocean and the atmosphere, because of, for example, increased sea-ice cover and changes in the large-scale overturning circulation, are likely to have further increased these values, especially at high latitudes. Indeed, where shallow sub-surface reservoir age estimates are available for the LGM, they are typically significantly higher than the modern values[21,22,25,42,46–48].

Despite the challenges involved in estimating past shallow sub-surface reservoir age variability, it is clear that ignoring them entirely is not a viable option, especially in a study that seeks to constrain past ocean circulation changes.

Recent work on core MD09-3257, from the Brazil Margin, showed that an independent calendar age model could be established for that core using U-Th dated speleothem records on the adjacent continent[49], based on the fact that increased precipitation is marked by a decrease in δ^{18}O in South American speleothems[50,51] and increased sedimentary Ti/Ca ratios in marine sediment cores off the northeastern Brazilian coast[52]. However, because of a lack of available calendar age tie points for the LGM, surface reservoir ages based on this calendar age-scale remain sparse. We therefore adopt an estimate for LGM surface reservoir ages on the Brazil Margin based on the modern reservoir age corrected for pCO_2-dependent air–sea gas exchange effects[44,45]. A reservoir age of 750 years (250 years greater than modern), which would have arisen due to globally reduced air–sea gas exchange rates, is used. Because it is unclear how ocean circulation changes may have affected this region we apply large uncertainties to this estimate of ±250 years. By combining high-resolution radiocarbon dating with calendar age models of centennial precision, it may be possible to reduce this uncertainty in the future.

Because the Iberian Margin cores contain a very clear event stratigraphy[53,54], these cores were stratigraphically aligned to the uranium-series dated speleothem records from Hulu Cave[55] and the layer counted (GICC05) NGRIP dust record[56,57] using the Zr/Sr ratio determined using X-ray fluorescence (XRF; see Supplementary Figs 2 and 3). The cores were aligned to both the Hulu speleothem and NGRIP simultaneously using a series of tie points including two tie-points within the LGM (18–23 1000 years before present (kyrs BP)). Shallow sub-surface reservoir ages were determined directly by subtracting the planktonic age from the contemporaneous atmospheric age, using the calendar ages obtained at tie-points, and the atmospheric radiocarbon calibration curve IntCal13 (ref. 58; Supplementary Table 3). LGM surface reservoir ages on the Iberian Margin are thus estimated to be around 900 years with upper and lower limits of 1,100 years and 700 years, respectively. These ages are consistent with the lowest estimates determined for the Iberian Margin by ref. 22 (that is, excluding their tie-points in HS1 and the LGM where the event stratigraphy is arguably more equivocal).

Age models. The planktonic radiocarbon ages were used to construct age models for each of the cores. In order to do so, an estimated surface reservoir age was subtracted from each planktonic radiocarbon date before conversion to calendar ages using BChron version 3.1.5 (ref. 59) and the IntCal13 calibration curve[58]. These calendar ages were then used to construct sediment depth-age models using the Markov Chain Monte-Carlo method, also using Bchron. As LGM surface reservoir age estimates have not been directly estimated on the Brazil Margin, a 'best guess' value of 750 years, based on isotope exchange constraints backed up by model simulations[44,45], was used. For the Iberian Margin, a surface reservoir age of 900 years was used for the LGM based on the stratigraphic alignments described above.

For compiled data, for cores with age models that do not depend on radiocarbon data, surface and deep reservoir ages were determined by subtracting the contemporary atmospheric radiocarbon age (based on Intcal13) from the planktonic and benthic radiocarbon ages, respectively. For sites with no independent age model, the pCO_2 corrected modern reservoir ages (that is, modern plus 250 years at the LGM) were used and added to the benthic-planktonic age offset to determine the deep ocean-atmospheric age offset (Supplementary Table 2).

Stratigraphic alignments. The cores were stratigraphically aligned to the Hulu speleothem $\delta^{18}O$ record[55] and the NGRIP dust record[57] (on the GICC05 age model[56,60]). The NGRIP dust content changes rapidly and synchronously with changes in ice core $\delta^{18}O$ (ref. 61). NGRIP dust, which is predominantly sourced from East Asian deserts[62–65], increases during cold periods[57]. These increases are caused by atmospheric changes[66,67] and/or intensified sources[68], but the exact mechanism is unconstrained. The Hulu speleothem $\delta^{18}O$ record resembles East Asian monsoon changes and is highly correlated with millennial scale Greenland temperature variations[55,69].

The sediment cores were aligned using elemental ratios determined using high-resolution XRF. Zr/Sr ratios were used to align the Iberian Margin cores. Zr/Sr anti-correlates strongly with Ca/Ti in these cores. The Zr/Sr and Ca/Ti ratios reflect the relative input of biogenic (Ca, Sr) and detrital (Zr, Ti) material, and have been shown to correlate strongly with planktonic $\delta^{18}O$ and alkenone sea-surface temperatures on the Iberian Margin, as well as with millennial scale variations in Greenland ice core $\delta^{18}O$ (ref. 70). Zr/Sr values are generally higher during stadials and lower during interstadials, whereas Ca/Ti ratios show the opposite trend.

A master core, SHAK03-6K was selected for the Iberian Margin through which the other cores were aligned. SHAK03-6K was chosen as the master core based on its high quality (no discontinuities) and age range (SHAK14-4G was also of very high quality but only reached back to ~20 kyrs). SHAK03-6K was aligned to both the Hulu speleothem and the NGRIP dust record using a series of tie points (Supplementary Fig. 2). No tie-points were used in the interval 0–11.4 kyrs BP because of the lack of clear signals in the records. The calendar ages at tie points in SHAK03-6K were then transferred to all the other Iberian Margin cores (Supplementary Fig. 3).

XRF data. The Iberian Margin cores were scanned at the University of Cambridge using an Avaatech XRF core scanner (2nd generation). The surface of the cores was scraped clean then covered with a 4-μm SPEXCertiPrep Ultralene foil to avoid contamination and to prevent the cores drying out and cracking. Each section was measured at three different voltages and currents: 10 kV and 750 μA, 30 kV and 500 μA, and at 50 kV and 1,000 μA. The entire length of each core was analysed at 5-mm resolution with an irradiated surface length and width of 5 mm (downcore) and 12 mm (cross core), respectively. The count time was 60 s for each measurement. Element intensities were obtained by post-processing of the XRF spectra using the Canberra WinAxil software with standard software settings and spectrum-fit models.

Data availability. The data supporting the findings of this study are available within the article and its Supplementary Information files.

References

1. Boyle, E. A. & Keigwin, L. D. Deep Circulation of the North Atlantic over the Last 200,000 Years: geochemical Evidence. *Science* **218,** 784–787 (1982).
2. Duplessy, J. C. *et al.* Deep water source variations during the last climatic cycle and their impact on the global deep water circulation. *Paleoceanography* **3,** 343–360 (1988).
3. Curry, W. & Oppo, D. Glacial water mass geometry and the distribution of $\delta^{13}C$ of Sigma CO_2 in the western Atlantic Ocean. *Paleoceanography* **20,** PA1017 (2005).
4. Marchitto, T. M. & Broecker, W. S. Deep water mass geometry in the glacial Atlantic Ocean: a review of constraints from the paleonutrient proxy Cd/Ca. *Geochem. Geophys. Geosystems* **7,** Q12003 (2006).
5. Lynch-Stieglitz, J. *et al.* Atlantic meridional overturning circulation during the Last Glacial Maximum. *Science* **316,** 66–69 (2007).
6. Lund, D. C., Mix, A. C. & Southon, J. Increased ventilation age of the deep northeast Pacific Ocean during the last deglaciation. *Nat. Geosci.* **4,** 771–774 (2011).
7. Oppo, D. W. & Lehman, S. J. Mid-depth circulation of the subpolar North Atlantic during the Last Glacial Maximum. *Science* **259,** 1148–1152 (1993).
8. Gebbie, G. How much did Glacial North Atlantic Water shoal? *Paleoceanography* **29,** 190–209 (2014).
9. Gebbie, G., Peterson, C. D., Lisiecki, L. E. & Spero, H. J. Global-mean marine ^{13}C and its uncertainty in a glacial state estimate. *Quat. Sci. Rev.* **125,** 144–159 (2015).
10. Lippold, J. *et al.* Strength and geometry of the glacial Atlantic Meridional Overturning Circulation. *Nat. Geosci.* **5,** 813–816 (2012).
11. McManus, J. F., Francois, R., Gherardi, J.-M., Keigwin, L. D. & Brown-Leger, S. Collapse and rapid resumption of Atlantic meridional circulation linked to deglacial climate changes. *Nature* **428,** 834–837 (2004).
12. Keigwin, L. D. & Boyle, E. A. Did North Atlantic overturning halt 17,000 years ago? *Paleoceanography* **23,** PA1101 (2008).
13. Sarnthein, M., Schneider, B. & Grootes, P. M. Peak glacial ^{14}C ventilation ages suggest major draw-down of carbon into the abyssal ocean. *Clim. Past* **9,** 2595–2614 (2013).
14. Zahn, R., Sarnthein, M. & Erlenkeuser, H. Benthic isotope evidence for changes of the Mediterranean outflow during the Late Quaternary. *Paleoceanography* **2,** 543–559 (1987).
15. Charles, C. D. & Fairbanks, R. G. Evidence from Southern Ocean sediments for the effect of North Atlantic deep-water flux on climate. *Nature* **355,** 416–416 (1992).
16. Ninnemann, U. S. & Charles, C. D. Changes in the mode of Southern Ocean circulation over the last glacial cycle revealed by foraminiferal stable isotopic variability. *Earth Planet. Sci. Lett.* **201,** 383–396 (2002).
17. Boyle, E. & Keigwin, L. North Atlantic thermohaline circulation during the past 20,000 years linked to high-latitude surface temperature. *Nature* **330,** 35–40 (1987).
18. Keigwin, L. D. Radiocarbon and stable isotope constraints on Last Glacial Maximum and Younger Dryas ventilation in the western North Atlantic. *Paleoceanography* **19,** PA4012 (2004).
19. Cléroux, C., Demenocal, P. & Guilderson, T. Deglacial radiocarbon history of tropical Atlantic thermocline waters: absence of CO_2 reservoir purging signal. *Quat. Sci. Rev.* **30,** 1875–1882 (2011).
20. Barker, S., Knorr, G., Vautravers, M. J., Diz, P. & Skinner, L. C. Extreme deepening of the Atlantic overturning circulation during deglaciation. *Nat. Geosci.* **3,** 567–571 (2010).
21. Skinner, L. C., Fallon, S., Waelbroeck, C., Michel, E. & Barker, S. Ventilation of the deep southern ocean and deglacial CO_2 rise. *Science* **328,** 1147–1151 (2010).
22. Skinner, L. C., Waelbroeck, C., Scrivner, A. E. & Fallon, S. J. Radiocarbon evidence for alternating northern and southern sources of ventilation of the deep Atlantic carbon pool during the last deglaciation. *Proc. Natl Acad. Sci. USA* **111,** 5480 (2014).
23. Sortor, R. N. & Lund, D. C. No evidence for a deglacial intermediate water [DELTA]^{14}C anomaly in the SW Atlantic. *Earth Planet. Sci. Lett.* **310,** 65 (2011).
24. Keigwin, L. D. & Schlegel, M. A. Ocean ventilation and sedimentation since the glacial maximum at 3 km in the western North Atlantic. *Geochem. Geophys. Geosystems* **3,** 1034 (2002).
25. Burke, A. & Robinson, L. F. The Southern Ocean's role in carbon exchange during the last deglaciation. *Science* **335,** 557–561 (2012).
26. Matsumoto, K. Radiocarbon-based circulation age of the world oceans. *J. Geophys. Res. Oceans* **112,** C09004 (2007).
27. Orsi, A. H., Johnson, G. C. & Bullister, J. L. Circulation, mixing, and production of Antarctic Bottom Water. *Prog. Oceanogr.* **43,** 55–109 (1999).
28. Gutjahr, M., Frank, M., Stirling, C. H., Keigwin, L. D. & Halliday, A. N. Tracing the Nd isotope evolution of North Atlantic Deep and intermediate waters in the western North Atlantic since the Last Glacial Maximum from Blake Ridge sediments. *Earth Planet. Sci. Lett.* **266,** 61–77 (2008).
29. Otto-Bliesner, B. L. *et al.* Last Glacial Maximum ocean thermohaline circulation: PMIP2 model intercomparisons and data constraints. *Geophys. Res. Lett.* **34,** L12706 (2007).
30. Chikamoto, M. O. *et al.* Variability in North Pacific intermediate and deep water ventilation during Heinrich events in two coupled climate models. *Deep Sea Res. Part II* **61-64,** 114–126 (2012).
31. Ferrari, R. *et al.* Antarctic sea ice control on ocean circulation in present and glacial climates. *Proc. Natl. Acad. Sci. USA* **111,** 8753–8758 (2014).
32. Ito, T. & Follows, M. J. Preformed phosphate, soft tissue pump and atmospheric CO_2. *J. Mar. Res.* **63,** 813–839 (2005).
33. Ito, T. & Follows, M. J. Air-sea disequilibrium of carbon dioxide enhances the biological carbon sequestration in the Southern Ocean. *Glob. Biogeochem. Cycles* **27,** 1129–1138 (2013).
34. Freeman, E. *et al.* An Atlantic-Pacific ventilation seesaw across the last deglaciation. *Earth Planet. Sci. Lett.* **424,** 237–244 (2015).
35. Freeman, E., Skinner, L. C., Reimer, R., Scrivner, A. E. & Fallon, S. Graphitization of small carbonate samples for palaeoceanographic research at the Godwin Radiocarbon Laboratory, University of Cambridge. *Radiocarbon* **58,** 89–97 (2015).
36. Stuiver, M. & Polach, H. Reporting of ^{14}C data. *Radiocarbon* **19,** 355–363 (1977).
37. Cook, M. S. & Keigwin, L. D. Radiocarbon profiles of the NW Pacific from the LGM and deglaciation: evaluating ventilation metrics and the effect of uncertain surface reservoir ages. *Paleoceanography* **30,** 174–195 (2015).
38. Key, R. M. *et al.* A global ocean carbon climatology: results from Global Data Analysis Project (GLODAP). *Glob. Biogeochem. Cycles* **18,** GB4031 (2004).

39. De Pol-Holz, R., Keigwin, L., Southon, J., Hebbeln, D. & Mohtadi, M. No signature of abyssal carbon in intermediate waters off Chile during deglaciation. *Nat. Geosci.* **3,** 192–195 (2010).
40. Max, L. *et al.* Pulses of enhanced North Pacific Intermediate Water ventilation from the Okhotsk Sea and Bering Sea during the last deglaciation. *Clim. Past* **10,** 591–605 (2014).
41. Govin, A. *et al.* Evidence for northward expansion of Antarctic Bottom Water mass in the Southern Ocean during the last glacial inception. *Paleoceanography* **24,** PA1202 (2009).
42. de la Fuente, M., Skinner, L., Calvo, E., Pelejero, C. & Cacho, I. Increased reservoir ages and poorly ventilated deep waters inferred in the glacial Eastern Equatorial Pacific. *Nat. Commun* **6,** 7420 (2015).
43. Lindsay, C. M., Lehman, S. J., Marchitto, T. M. & Ortiz, J. D. The surface expression of radiocarbon anomalies near Baja California during deglaciation. *Earth Planet. Sci. Lett.* **422,** 67–74 (2015).
44. Butzin, M., Prange, M. & Lohmann, G. Readjustment of glacial radiocarbon chronologies by self-consistent three-dimensional ocean circulation modeling. *Earth Planet. Sci. Lett.* **317-318,** 177–184 (2012).
45. Galbraith, E. D., Kwon, E. Y., Bianchi, D., Hain, M. P. & Sarmiento, J. L. The impact of atmospheric pCO_2 on carbon isotope ratios of the atmosphere and ocean. *Glob. Biogeochem. Cycles* **29,** 307–324 (2015).
46. Sikes, E. L., Samson, C. R., Guilderson, T. P. & Howard, W. R. Old radiocarbon ages in the southwest Pacific Ocean during the last glacial period and deglaciation. *Nature* **405,** 555–559 (2000).
47. Waelbroeck, C. *et al.* The timing of the last deglaciation in North Atlantic climate records. *Nature* **412,** 724–727 (2001).
48. Skinner, L. *et al.* Reduced ventilation and enhanced magnitude of the deep Pacific carbon pool during the last glacial period. *Earth Planet. Sci. Lett.* **411,** 45–52 (2015).
49. Burckel, P. *et al.* Atlantic Ocean circulation changes preceded millennial tropical South America rainfall events during the last glacial. *Geophys. Res. Lett.* **42,** 411–418 (2015).
50. Cheng, H. *et al.* Climate change patterns in Amazonia and biodiversity. *Nat. Commun.* **4,** 1411–1411 (2013).
51. Cruz, F. W. *et al.* Orbitally driven east-west antiphasing of South American precipitation. *Nat. Geosci.* **2,** 210–214 (2009).
52. Jaeschke, A., Rühlemann, C., Arz, H., Heil, G. & Lohmann, G. Coupling of millennial-scale changes in sea surface temperature and precipitation off northeastern Brazil with high-latitude climate shifts during the last glacial period. *Paleoceanography* **22,** PA4206 (2007).
53. Shackleton, N. J. The 100,000-year ice-age cycle identified and found to lag temperature, carbon dioxide, and orbital eccentricity. *Science* **289,** 1897–1902 (2000).
54. Skinner, L. C., Elderfield, H. & Hall, M. in *Ocean Circulation: Mechanisms and Impacts'Past and Future Changes of Meridional Overturning* 197–208 (American Geophysical Union, 2007).
55. Southon, J., Noronha, A. L., Cheng, H., Edwards, R. L. & Wang, Y. A high-resolution record of atmospheric 14C based on Hulu Cave speleothem H82. *Quat. Sci. Rev.* **33,** 32 (2012).
56. Andersen, K. K. *et al.* The Greenland Ice Core Chronology 2005, 15ka. Part 1: constructing the time scale. *Quat. Sci. Rev.* **25,** 3246–3257 (2006).
57. Ruth, U., Wagenbach, D., Steffensen, J. P. & Bigler, M. Continuous record of microparticle concentration and size distribution in the central Greenland NGRIP ice core during the last glacial period. *J. Geophys. Res. Atmospheres* **108,** 4098 (2003).
58. Reimer, P. *et al.* IntCal13 and Marine13 Radiocarbon Age Calibration Curves 0–50,000 Years cal BP. *Radiocarbon* **55,** 1869–1887 (2013).
59. Parnell, A. C., Haslett, J., Allen, J. R. M., Buck, C. E. & Huntley, B. A flexible approach to assessing synchroneity of past events using Bayesian reconstructions of sedimentation history. *Quat. Sci. Rev.* **27,** 1872–1885 (2008).
60. Rasmussen, S. O. *et al.* A new Greenland ice core chronology for the last glacial termination. *J. Geophys. Res. Atmospheres* **111,** D06102 (2006).
61. Ruth, U. *et al.* Ice core evidence for a very tight link between North Atlantic and east Asian glacial climate. *Geophys. Res. Lett.* **34,** L03706 (2007).
62. Biscaye, P. *et al.* Asian provenance of glacial dust (stage 2) in the Greenland Ice Sheet Project 2 Ice Core, Summit, Greenland. *J. Geophys. Res. Oceans* **102,** 26765–26781 (1997).
63. Kahl, J. D. W. *et al.* Air mass trajectories to Summit, Greenland: a 44-year climatology and some episodic events. *J. Geophys. Res.* **102,** 26861–26875 (1997).
64. Svensson, A., Biscaye, P. & Grousset, F. Characterization of late glacial continental dust in the Greenland Ice Core Project ice core. *J. Geophys. Res.-Atmospheres* **105,** 4637–4656 (2000).
65. Bory, A. J., Biscaye, P. E., Svensson, A. & Grousset, F. E. Seasonal variability in the origin of recent atmospheric mineral dust at NorthGRIP, Greenland. *Earth Planet. Sci. Lett.* **196,** 123–134 (2002).
66. Petit, J. R., M, B. & A, R. Ice age aerosol content from East Antarctic ice core samples and past wind strength. *Nature* **293,** 391–394 (1981).
67. Petit, J. R. *et al.* Palaeoclimatological and chronological implications of the Vostok core dust record. *Nature* **343,** 56–58 (1990).
68. Fuhrer, K., Wolff, E. & Johnsen, S. Timescales for dust variability in the Greenland Ice Core Project (GRIP) ice core in the last 100,000 years. *J. Geophys. Res. Atmospheres* **104,** 31043–31052 (1999).
69. Wang, Y. J. *et al.* a high-resolution absolute-dated late pleistocene monsoon record from Hulu Cave, China. *Science* **294,** 2345–2348 (2001).
70. Hodell, D. *et al.* Response of Iberian Margin sediments to orbital and suborbital forcing over the past 420 ka. *Paleoceanography* **28,** 185–199 (2013).
71. Schlitzer, R. Ocean Data View http://odv.awi.de (2016).

Acknowledgements

We thank James Rolfe and Ian Mather for stable isotope measurements, Simon Crowhurst for XRF core scanning, and Ron Reimer for doing the AMS measurements. This work was made possible by NERC support for the cruise that collected the JC89-SHAK cores (NE/J00653X/1) and by NERC grant NE/L006421/1, as well as support from the Royal Society and the Isaac Newton Trust. MD09 cores were collected on board R/V Marion Dufresne during RETRO cruise III, supported by ESF EUROMARC project RETRO, IPEV and ANR project ANR-09-BLAN-0347. C.W. acknowledges support from the European Research Council grant ACCLIMATE/no 339108. This is LSCE contribution 5579.

Author contributions

E.F. and L.C.S. designed the study. L.C.S., D.H. and C.W. collected the core material. E.F. compiled the published data and obtained all the new data. E.F. and L.C.S. analysed the data. E.F. and L.C.S. wrote the manuscript with contributions from all authors.

Additional information

Supplementary Information accompanies this paper at http://www.nature.com/naturecommunications

Competing financial interests: The authors declare no competing financial interests.

Reprints and permission information is available online at http://npg.nature.com/reprintsandpermissions/

How to cite this article: Freeman, E. *et al.* Radiocarbon evidence for enhanced respired carbon storage in the Atlantic at the Last Glacial Maximum. *Nat. Commun.* 7:11998 doi: 10.1038/ncomms11998 (2016).